Chiral symmetry restoration in linear sigma models with different numbers of quark flavors

Dirk Röder,* Jörg Ruppert,[†] and Dirk H. Rischke[‡]

Institut für Theoretische Physik, Johann Wolfgang Goethe-Universität, Robert-Mayer-Str. 8–10, D-60054 Frankfurt/Main, Germany
(Received 28 January 2003; published 3 July 2003)

Chiral symmetry restoration at nonzero temperature is studied in the framework of the $O(4)$ linear sigma model and the $U(N_f)_r \times U(N_f)_\ell$ linear sigma model with $N_f = 2$, 3 and 4 quark flavors. We investigate the temperature dependence of the masses of the scalar and pseudoscalar mesons, and the nonstrange, strange, and charm condensates within the Hartree approximation as derived from the Cornwall-Jackiw-Tomboulis formalism. We find that the masses of the nonstrange and strange mesons at nonzero temperature depend sensitively on the particular symmetry of the model and the number of light quark flavors N_f. On the other hand, because of the large charm quark mass, neither do charmed mesons significantly affect the properties of the other mesons, nor do their masses change appreciably in the temperature range around the chiral symmetry restoration temperature. In the chiral limit, the transition temperatures for chiral symmetry restoration are surprisingly close to those found in lattice QCD.

I. INTRODUCTION

For N_f massless quark flavors, the QCD Lagrangian has a chiral $U(N_f)_r \times U(N_f)_\ell = SU(N_f)_r \times SU(N_f)_\ell \times U(1)_V \times U(1)_A$ symmetry. Here, $V = r + \ell$, while $A = r - \ell$. The $U(1)_V$ symmetry corresponds to baryon number conservation. It is always respected and thus plays no role in the symmetry breaking patterns considered in the following. In the vacuum, a nonvanishing expectation value of the quark condensate, $\langle \bar{q}_\ell q_r \rangle \neq 0$, spontaneously breaks the above symmetry to $SU(N_f)_V$. This gives rise to N_f^2 Goldstone bosons which dominate the low-energy dynamics of the theory. As shown by 't Hooft [1,2], instantons break the $U(1)_A$ symmetry explicitly to $Z(N_f)_A$ [3]. (For the low-energy dynamics of QCD, however, this discrete symmetry is irrelevant.) Consequently, one of the N_f^2 Goldstone bosons becomes massive, leaving $N_f^2 - 1$ Goldstone bosons. The $SU(N_f)_r \times SU(N_f)_\ell \times U(1)_A$ symmetry of the QCD Lagrangian is also explicitly broken by nonzero quark masses. The $N_f^2 - 1$ low-energy degrees of freedom then become pseudo-Goldstone bosons. For $M \leq N_f$ degenerate quark flavors, an $SU(M)_V$ symmetry is preserved.

As indicated by lattice QCD calculations [4], chiral symmetry is restored at temperatures around ~ 150 MeV (at zero net-baryon number density). It is difficult to determine the order of the chiral phase transition on the lattice. At this time, lattice calculations have not unambiguously answered this question. For physical values of the quark masses, calculations with staggered fermions [5] favor a smooth crossover transition, while calculations with Wilson fermions [6] predict the transition to be of first order.

For vanishing quark masses, i.e., in the chiral limit, however, one can use universality arguments to determine the order of the phase transition. According to universality, the order of the chiral transition in QCD is identical to that in a

theory with the same chiral symmetries as QCD, for instance, the $U(N_f)_r \times U(N_f)_\ell$ linear sigma model. This argument was employed by Pisarski and Wilczek [3] who found that for $N_f = 2$ flavors of massless quarks, the transition can be of second order, if the $U(1)_A$ symmetry is explicitly broken by instantons. It is driven first order by fluctuations, if the $U(1)_A$ symmetry is restored at T_c. For $N_f = 3$ massless flavors, the transition is always first order. In this case, the term which breaks the $U(1)_A$ symmetry explicitly is a cubic invariant, and consequently drives the transition first order. In the absence of explicit $U(1)_A$ symmetry breaking, the transition is fluctuation-induced of first order. For $N_f = 4$, the same argument leads to a first order chiral transition in the absence of the $U(1)_A$ anomaly. The term which breaks the $U(1)_A$ symmetry is no longer a cubic invariant, but of quartic order in the fields. Since this term does not generate an infrared-stable fix point, the transition remains of first order.

For nonzero quark masses, the chiral symmetry of QCD is explicitly broken. Nonzero quark masses act like a magnetic field in spin systems, such that a second order phase transition becomes a crossover transition. When the quark masses increase, a first order phase transition may for a while remain of first order, but it will ultimately become a crossover transition, too. In order to decide whether this happens for a particular choice of quark masses, universality arguments cannot be applied and one has to resort to numerical calculations. As an alternative to lattice QCD calculations, one can also use linear sigma models to investigate this question [7].

Studying the linear sigma model at nonzero temperature, however, requires many-body resummation schemes, because infrared divergences cause naive perturbation theory to break down [8]. In these resummation schemes, one necessarily has to make approximations by selecting certain subsets of diagrams. The most commonly employed scheme is the Hartree approximation. This approximation fails to reproduce the correct order of the chiral transition for the $O(4)$ linear sigma model: the transition is of second order, while the Hartree approximation yields a first order transition. For $U(N_f)_r \times U(N_f)_\ell$ linear sigma models with $N_f = 3$, however, the Hartree approximation correctly produces a first order chiral transition [9]. For $N_f = 2$, in the absence of the $U(1)_A$

*Electronic address: roeder@th.physik.uni-frankfurt.de
†Electronic address: ruppert@th.physik.uni-frankfurt.de
‡Electronic address: drischke@th.physik.uni-frankfurt.de

TABLE I. The table shows the symmetry breaking patterns studied in this paper. The $\sqrt{}$ symbol indicates that the specific symmetry breaking pattern is physically interesting and investigated here. The $\times$ symbol indicates that this symmetry breaking pattern does not exist at all and the $-$ symbolizes that the respective symmetry breaking pattern is not studied.

	$O(4)$	$U(2)_r \times U(2)_\ell$	$U(3)_r \times U(3)_\ell$	$U(4)_r \times U(4)_\ell$
Explicit chiral symmetry breaking with $U(1)_A$ anomaly	$\sqrt{}$	$\sqrt{}$	$\sqrt{}$	$\sqrt{}$
Explicit chiral symmetry breaking without $U(1)_A$ anomaly	$\times$	$\sqrt{}$	$\sqrt{}$	$-$
Chiral limit with $U(1)_A$ anomaly	$\sqrt{}$	$\sqrt{}$	$\sqrt{}$	$-$
Chiral limit without $U(1)_A$ anomaly	$\times$	$\sqrt{}$	$\sqrt{}$	$-$

anomaly the transition is of first order and, as will be shown in this paper, the Hartree approximation agrees with this result. With the $U(1)_A$ anomaly, the transition is of second order. We shall find that the Hartree approximation (slightly) violates this prediction by producing a (weak) first order transition.

The utility of linear sigma models, however, transcends further than just predicting the order of the chiral phase transition. The degrees of freedom of the $U(N_f)_r \times U(N_f)_\ell$ linear sigma model are the scalar and pseudoscalar mesons. In the vacuum, the latter are the (pseudo-) Goldstone bosons of chiral symmetry breaking. Thus, the linear sigma model can also be viewed as an effective low-energy theory for QCD. At high temperatures, chiral symmetry is restored. Consequently, chiral partners among the scalar and pseudoscalar mesons must become degenerate in mass. Since the $U(N_f)_r \times U(N_f)_\ell$ linear sigma model treats both scalar and pseudoscalar mesons on the same footing, it is particularly suited to describe the change of meson properties across the chiral transition. Note that, in the case of a first order chiral transition which coincides with the deconfinement transition, the correct degrees of freedom in the high-temperature phase are quark and gluons instead of mesons. However, in the case of a crossover transition mesonic degrees of freedom are well-defined even above the chiral transition temperature. These arguments constitute the motivation for the present work. Let us briefly outline the contents of this paper. We investigate the change of meson masses and quark condensates with temperature in the framework of $U(N_f)_r \times U(N_f)_\ell$ linear sigma models. We focus in particular on the question how the number of quark flavors N_f changes the temperature dependence of the meson masses and the quark condensates. For a given N_f, we furthermore investigate the different patterns of symmetry breaking arising from the presence or absence of the $U(1)_A$ anomaly, and from taking

zero or nonzero values for the quark masses. In this sense, the present study is an extension of previous work [9,10]. Table I presents an overview of the different models and patterns of symmetry breaking studied in this paper.

The $U(2)_r \times U(2)_\ell$ linear sigma model has eight degrees of freedom: the scalar fields are the σ meson and the three a_0 mesons, the pseudoscalar fields are the η meson and the three pions. With spontaneous breaking of the $U(2)_A$ chiral symmetry, but without the $U(1)_A$ anomaly, the pions and the η meson are (pseudo-) Goldstone bosons, while the σ and a_0 meson are heavy states. With the $U(1)_A$ anomaly, the η meson also becomes heavy.

With the explicit breaking of the $U(1)_A$ symmetry due to the anomaly [and neglecting the $U(1)_V$ symmetry of baryon number conservation], the remaining symmetry of the $U(2)_r \times U(2)_\ell$ linear sigma model is $SU(2)_r \times SU(2)_\ell$. This group is isomorphic to $O(4)$. The appropriate effective theory incorporating this symmetry is the $O(4)$ linear sigma model [11]. This model has only four degrees of freedom, the σ meson and the three pions. In this sense, it represents the limit of the $U(2)_r \times U(2)_\ell$ model for maximum $U(1)_A$ symmetry breaking. The $U(2)_r \times U(2)_\ell$ model is more general, since it allows us to consider the properties of mesons also without the $U(1)_A$ anomaly.

In the limit of maximum $U(1)_A$ symmetry breaking, the η and a_0 mesons become infinitely heavy and are thus removed from the spectrum of physical excitations. This approximation is justified at small temperatures, where the dynamics is determined by the lightest hadronic degrees of freedom, i.e., the pions and, to some extent, the σ meson. At higher temperatures and, in particular, around the chiral transition, however, heavier mesons become more and more important. It is therefore interesting to compare the results of the $O(4)$ model with those of the $U(2)_r \times U(2)_\ell$ model

which incorporates these heavier degrees of freedom. Note that the $O(4)$ linear sigma model at nonzero temperature has been discussed in Refs. [10,12].

In the physical hadron spectrum, the kaons are lighter than the a_0 and η mesons and thus are more copiously produced at nonzero temperature. Consequently, the kaons are expected to influence the dynamics of the system to a larger extent than the a_0 and η mesons. Therefore, the $U(2)_r \times U(2)_\ell$ model is unrealistic in the sense that it neglects these strange meson degrees of freedom. From a physical point of view, it is thus necessary to enlarge the symmetry group to $U(3)_r \times U(3)_\ell$ and study the corresponding linear sigma model. Nevertheless, it is still interesting to compare the $U(2)_r \times U(2)_\ell$ model with the $U(3)_r \times U(3)_\ell$ model in order to see how the strange degrees of freedom affect the results. The $U(3)_r \times U(3)_\ell$ model was previously studied at nonzero temperature in Ref. [9].

Finally, we extend our investigations by including the charm degree of freedom. In principle, the corresponding linear sigma model has an $SU(4)_r \times SU(4)_\ell \times U(1)_A$ symmetry, but in nature this symmetry is strongly explicitly broken by the large charm quark mass. Therefore, we only consider the physically relevant case of explicit chiral symmetry breaking with $U(1)_A$ anomaly.

For all cases considered (see Table I) we study the meson masses and the condensates as functions of temperature. In the chiral limit, we determine the phase transition temperatures by computing the effective potentials. In this aspect, we extend the previous study of Ref. [9]. For the $O(4)$ model, this has already been done in Ref. [12].

Our calculations are done in the Hartree approximation which we derive within the Cornwall-Jackiw-Tomboulis (CJT) formalism [13]. The Hartree approximation has the advantage that the meson self-energies become independent of momentum and energy and one only has to solve gap equations for the meson masses as a function of temperature. To go beyond the Hartree approximation, for instance by including energy-momentum-dependent contributions to the self-energies, is considerably more difficult [14–17], and will be deferred to a future publication.

The remainder of this paper is organized as follows. In Sec. II we review the formulas of the CJT formalism, which are relevant for the present study, and apply them to the $O(4)$ model and the $U(N_f)_r \times U(N_f)_\ell$ linear sigma models for $N_f = 2$, 3, and 4. In Sec. III it is shown how to determine the coupling constants of the different models from the vacuum properties of the mesons and condensates. In Sec. IV we discuss the temperature dependence of the masses and the condensates. We conclude this work in Sec. V with a summary of our results.

We use the imaginary-time formalism to compute quantities at nonzero temperature. Our notation is

$$\int_k f(k) \equiv T \sum_{n=-\infty}^{\infty} \int \frac{d^3\mathbf{k}}{(2\pi)^3} f(2\pi i n T, \mathbf{k}), \quad (1)$$

$$\int_x f(x) \equiv \int_0^{1/T} d\tau \int d^3\mathbf{x} f(\tau, \mathbf{x}).$$

Our units are $\hbar = c = k_B = 1$. The metric tensor is $g^{\mu\nu} = \mathrm{diag}(+, -, -, -)$. Throughout this work, all latin subscripts are adjoint $U(N_f)$ indices, $a = 0, \ldots, N_f^2 - 1$, and a summation over repeated indices is understood.

II. LINEAR SIGMA MODELS IN THE HARTREE APPROXIMATION

A. The CJT formalism

The CJT formalism [13] generalizes the concept of the effective action for one-point functions to that of an effective action for one- and two-point functions. It is particularly useful for theories with spontaneously broken symmetry. In this case, truncating the standard loop expansion for the effective action [18] at some given order, at nonzero temperature one may obtain unphysical, tachyonic propagation of quasiparticles with small momenta. The reason for this failure of the standard loop expansion is that only the expectation value of the one-point function is self-consistently determined in this approach. The CJT formalism goes beyond the standard loop expansion by self-consistently determining the expectation value for the two-point function in addition to that of the one-point function. Effectively, this amounts to solving a Dyson-Schwinger equation for the two-point functions and yields a self-consistent computation of the quasiparticle self-energy. For translationally invariant systems, the effective action becomes the effective potential. To give an example, consider the general Lagrangian

$$\mathcal{L}(\varphi) = \frac{1}{2} \partial_\mu \varphi \partial^\mu \varphi - U(\varphi) \quad (2)$$

for a scalar quantum field φ. The effective potential in the CJT formalism reads

$$V[\bar{\phi}, \bar{G}] = U(\bar{\phi}) + \frac{1}{2} \int_k \ln \bar{G}^{-1}(k)$$

$$+ \frac{1}{2} \int_k [G^{-1}(k; \bar{\phi}) \bar{G}(k) - 1] + V_2[\bar{\phi}, \bar{G}], \quad (3)$$

where $\bar{\phi}$ is a c-number field (it is the expectation value of the quantum field φ in the presence of an external source), $U(\bar{\phi})$ is the classical potential energy density (the tree-level potential) in the Lagrangian (2), and G^{-1} is the inverse of the tree-level propagator,

$$G^{-1}(k; \bar{\phi}) \equiv -k^2 + U''(\bar{\phi}). \quad (4)$$

Here, $U''(\bar{\phi})$ is the second derivative of $U(\bar{\phi})$ with respect to $\bar{\phi}$. The last term in Eq. (3), $V_2[\bar{\phi}, \bar{G}]$, is the sum of all two-particle irreducible vacuum diagrams where all lines represent full propagators $\bar{G}$. The expectation values of the one-point function, ϕ, and of the two-point function, $\mathcal{G}(k)$, are determined from the stationarity conditions

$$\frac{\delta V[\bar{\phi}, \bar{G}]}{\delta \bar{\phi}} \bigg|_{\bar{\phi}=\phi, \bar{G}=\mathcal{G}} = 0, \tag{5a}$$

$$\frac{\delta V[\bar{\phi}, \bar{G}]}{\delta \bar{G}(k)} \bigg|_{\bar{\phi}=\phi, \bar{G}=\mathcal{G}} = 0. \tag{5b}$$

With Eq. (3), the latter can be written in the form

$$\mathcal{G}^{-1}(k) = G^{-1}(k; \phi) + \Pi(k), \tag{6a}$$

where

$$\Pi(k) \equiv 2 \frac{\delta V_2[\bar{\phi}, \bar{G}]}{\delta \bar{G}(k)} \bigg|_{\bar{\phi}=\phi, \bar{G}=\mathcal{G}} \tag{6b}$$

is the self-energy. Since $\Pi(k)$ is in general a functional of $\mathcal{G}$, Eq. (6a) represents a Schwinger-Dyson equation for the full (dressed) propagator.

The standard effective potential for the expectation value of the one-point function, $V(\bar{\phi})$, is obtained from the effective potential (3) by taking the full propagator $\bar{G}$ to be a function of $\bar{\phi}$, instead of an independent variable,

$$V(\bar{\phi}) = V[\bar{\phi}, \hat{G}(\bar{\phi})], \tag{7}$$

where $\hat{G}(k; \bar{\phi})$ is determined from

$$\frac{\delta V[\bar{\phi}, \bar{G}]}{\delta \bar{G}(k)} \bigg|_{\bar{G}=\hat{G}} = 0, \tag{8}$$

which is equivalent to

$$\hat{G}^{-1}(k; \bar{\phi}) = G^{-1}(k; \bar{\phi}) + \hat{\Pi}(k; \bar{\phi}), \tag{9a}$$

where

$$\hat{\Pi}(k; \bar{\phi}) \equiv 2 \frac{\delta V_2[\bar{\phi}, \bar{G}]}{\delta \bar{G}(k)} \bigg|_{\bar{G}=\hat{G}}. \tag{9b}$$

This expression and Eq. (3) can be used to obtain a compact form of the standard effective potential

$$V(\bar{\phi}) = U(\bar{\phi}) + \frac{1}{2} \int_k \ln \hat{G}^{-1}(k; \bar{\phi}) - \frac{1}{2} \int_k \hat{\Pi}(k; \bar{\phi}) \hat{G}(k; \bar{\phi})$$

$$+ V_2[\bar{\phi}, \hat{G}]. \tag{10}$$

Since V_2 contains infinitely many diagrams, an exact calculation is impossible. In practice, one has to restrict the computation of V_2 to a finite number of diagrams. The selected set of diagrams defines a particular many-body approximation. Cutting internal lines in these diagrams according to Eq. (6b), one obtains the diagrams contributing to the self-energy of the quasiparticles in this approximation scheme. Solving the Dyson-Schwinger equation (6a) provides a self-consistent calculation of this self-energy. In general, the
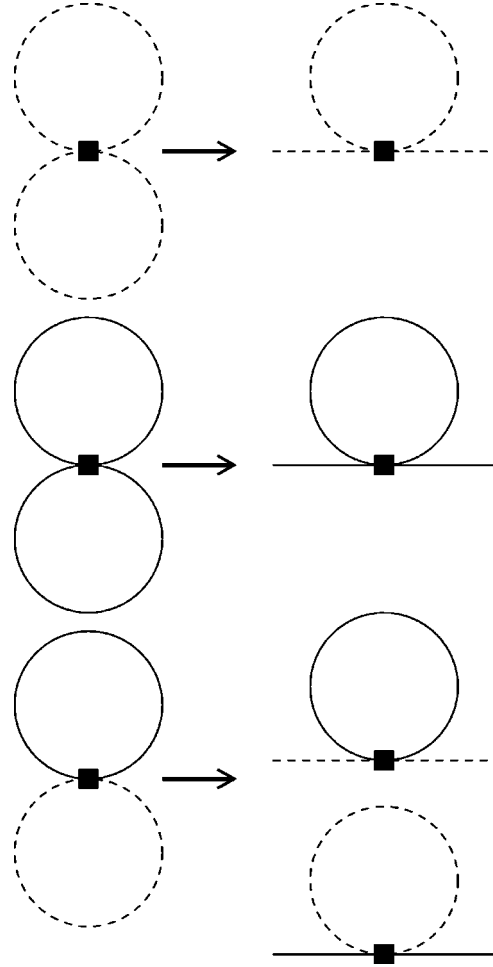

FIG. 1. Left-hand side: the double-bubble diagrams. Full lines are scalar particles, dashed lines are pseudoscalar particles. Right-hand side: the tadpole contributions to the self-energies obtained by cutting a line in the double-bubble diagrams on the left-hand side.

Dyson-Schwinger equation is an integral equation for the self-energy as a function of energy and momentum.

If one only takes the double-bubble diagrams on the left-hand side of Fig. 1 into account in the calculation of V_2, one obtains the Hartree approximation. Cutting these diagrams yields the well-known tadpole diagrams for the self-energy, cf. the right-hand side of Fig. 1. The Dyson-Schwinger equation (6a) is a self-consistency equation for this self-energy due to the fact that the internal lines in the tadpole diagrams represent full propagators. The Hartree approximation is a particularly simple many-body approximation scheme, because the tadpole diagrams are independent of energy and momentum, and thus the Dyson-Schwinger equations are no longer integral equations, but become fix-point equations for the quasiparticle masses.

B. The $O(4)$ model

In this section we apply the CJT formalism to the $O(N)$ model. Our numerical results presented in Sec. IV are exclusively for the case $N=4$. The CJT effective potential for the $O(N)$ model is [10]

$$V[\bar{\sigma},\bar{S},\bar{P}]=U(\bar{\sigma})+\frac{1}{2}\int_k[\ln \bar{S}^{-1}(k)+S^{-1}(k;\bar{\sigma})\bar{S}(k)-1]$$

$$+\frac{N-1}{2}\int_k[\ln \bar{P}^{-1}(k)+P^{-1}(k;\bar{\sigma})\bar{P}(k)-1]$$

$$+V_2[\bar{\sigma},\bar{S},\bar{P}], \tag{11}$$

where $\bar{\sigma}$ is the expectation value of the scalar field (in the presence of external sources). Because the vacuum of QCD has even parity, the expectation values of the pseudoscalar fields can be set to zero. The quantities $\bar{S}$ and $\bar{P}$ are the full propagators for scalar and pseudoscalar particles, while S^{-1} and P^{-1} are the corresponding inverse tree-level propagators,

$$S^{-1}(k;\bar{\sigma})=-k^2+m_\sigma^2(\bar{\sigma}), \tag{12a}$$

$$P^{-1}(k;\bar{\sigma})=-k^2+m_\pi^2(\bar{\sigma}), \tag{12b}$$

where the tree-level masses are

$$m_\sigma^2(\bar{\sigma})=\mu^2+\frac{12\lambda}{N}\bar{\sigma}^2, \tag{13a}$$

$$m_\pi^2(\bar{\sigma})=\mu^2+\frac{4\lambda}{N}\bar{\sigma}^2. \tag{13b}$$

The constant μ^2 is the bare mass term in the Lagrangian of the $O(N)$ model, while λ is the four-point coupling constant. For $\mu^2<0$, the $O(N)$ symmetry is spontaneously broken to $O(N-1)$, leading to $N-1$ Goldstone bosons. The tree-level potential is

$$U(\bar{\sigma})=\frac{1}{2}\mu^2\bar{\sigma}^2+\frac{\lambda}{N}\bar{\sigma}^4-H\bar{\sigma}, \tag{14}$$

where H is a term which breaks the $O(N)$ symmetry explicitly to $O(N-1)$. $V_2[\bar{\sigma},\bar{S},\bar{P}]$ is the sum of all two-particle irreducible diagrams. In the following, we restrict ourselves to the Hartree approximation, i.e., we take into account only the double-bubble diagrams shown on the left-hand side of Fig. 1. These diagrams have no explicit $\bar{\sigma}$ dependence. Then, only tadpole diagrams (with resummed propagators) contribute to the self-energies, cf. the right-hand side of Fig. 1. In the Hartree approximation,

$$V_2[\bar{S},\bar{P}]=3\frac{\lambda}{N}\left[\int_k\bar{S}(k)\right]^2+(N+1)(N-1)\frac{\lambda}{N}\left[\int_k\bar{P}(k)\right]^2$$

$$+2(N-1)\frac{\lambda}{N}\left[\int_k\bar{S}(k)\right]\left[\int_p\bar{P}(p)\right]. \tag{15}$$

The stationarity conditions (5a) and (5b) read

$$H=\mu^2\sigma+\frac{4\lambda}{N}\sigma^3+\frac{4\lambda}{N}\sigma\int_q[3\mathcal{S}(q)+(N-1)\mathcal{P}(q)], \tag{16a}$$

$$\mathcal{S}^{-1}(k)=-k^2+M_\sigma^2, \tag{16b}$$

$$\mathcal{P}^{-1}(k)=-k^2+M_\pi^2, \tag{16c}$$

where M_σ and M_π are the σ and pion masses dressed by contributions from the diagrams of Fig. 1,

$$M_\sigma^2=m_\sigma^2(\sigma)+\frac{4\lambda}{N}\left[3\int_q\mathcal{S}(q)+(N-1)\int_q\mathcal{P}(q)\right] \tag{17a}$$

$$M_\pi^2=m_\pi^2(\sigma)+\frac{4\lambda}{N}\left[\int_q\mathcal{S}(q)+(N+1)\int_q\mathcal{P}(q)\right]. \tag{17b}$$

Using Eqs. (17a) and (17b), Eq. (16a) can be written in the compact form

$$H=\sigma\left[M_\sigma^2-\frac{8\lambda}{N}\sigma^2\right]. \tag{17c}$$

Equations (17a), (17b), and (17c) are the stationarity conditions of the $O(N)$ model in the Hartree approximation. The explicit calculation of the tadpole integrals $\int_q\mathcal{S}(q)$ and $\int_q\mathcal{P}(q)$ will be discussed in Sec. II D.

C. The $U(N_f)_r\times U(N_f)_\ell$ linear sigma model for $N_f=2, 3$ and 4 flavors

The application of the CJT formalism to the $U(N_f)_r\times U(N_f)_\ell$ linear sigma model for $N_f=3$ was discussed in Ref. [9]. Since we want to treat the cases $N_f=2$ and $N_f=4$ on the same footing, we derive the CJT effective potential in somewhat greater detail than in the last section.

The Lagrangian of the $U(N_f)_r\times U(N_f)_\ell$ linear sigma model for $N_f=2,3$ or 4 flavors is given by [19–22]

$$\mathcal{L}(\Phi)=\text{Tr}(\partial_\mu\Phi^\dagger\partial^\mu\Phi-m^2\Phi^\dagger\Phi)-\lambda_1[\text{Tr}(\Phi^\dagger\Phi)]^2$$

$$-\lambda_2\text{Tr}(\Phi^\dagger\Phi)^2+c[\det(\Phi)+\det(\Phi^\dagger)]$$

$$+\text{Tr}[H(\Phi+\Phi^\dagger)]. \tag{18}$$

Φ is a complex $N_f\times N_f$ matrix parametrizing the scalar and pseudoscalar mesons,

$$\Phi=T_a\phi_a=T_a(\sigma_a+i\pi_a), \tag{19a}$$

where σ_a are the scalar ($J^P=0^+$) fields and π_a are the pseudoscalar ($J^P=0^-$) fields. The $N_f\times N_f$ matrix H breaks the symmetry explicitly and is chosen as

$$H=T_ah_a, \tag{19b}$$

where h_a are external fields. T_a are the generators of $U(N_f)$. The T_a are normalized such that $\text{Tr}(T_aT_b)=\delta_{ab}/2$. They obey the $U(N_f)$ algebra with

$$[T_a, T_b] = i f_{abc} T_c, \tag{20a}$$

$$\{T_a, T_b\} = d_{abc} T_c, \tag{20b}$$

where f_{abc} and d_{abc} are the standard antisymmetric and symmetric structure constants of $SU(N_f)$, $a, b, c = 1, \ldots, N_f^2 - 1$, and

$$f_{ab0} \equiv 0, \quad d_{ab0} \equiv \sqrt{\frac{2}{N_f}} \delta_{ab}. \tag{20c}$$

The terms in the first line of Eq. (18) are invariant under $U(N_f)_r \times U(N_f)_\ell \cong U(N_f)_V \times U(N_f)_A$ transformations. The determinant terms are invariant under $SU(N_f)_r \times SU(N_f)_\ell \cong SU(N_f)_V \times SU(N_f)_A$, but break the $U(1)_A$ symmetry explicitly. These terms arise from the $U(1)_A$ anomaly of the QCD vacuum. The last term in Eq. (18) breaks the axial and possibly the $SU(N_f)_V$ vector symmetries explicitly.

In the following we discuss the three different cases $N_f = 2$, 3, and 4 in detail. The identification of the σ_a and π_a fields with the physical scalar and pseudoscalar mesons is given in Appendix A.

A non-vanishing vacuum expectation value for Φ,

$$\langle \Phi \rangle \equiv T_a \bar{\sigma}_a, \tag{21}$$

breaks the chiral symmetry spontaneously. (If the vacuum does not break parity, the fields π_a cannot assume a non-vanishing vacuum expectation value.) Shifting the Φ field by this expectation value, the Lagrangian can be rewritten as

$$\mathcal{L} = \frac{1}{2} [\partial_\mu \sigma_a \partial^\mu \sigma_a + \partial_\mu \pi_a \partial^\mu \pi_a - \sigma_a (m_S^2)_{ab} \sigma_b$$
$$- \pi_a (m_P^2)_{ab} \pi_b] - \left[\frac{4}{3} \mathcal{F}_{abcd} \bar{\sigma}_d - \delta(N_f, 3) \mathcal{G}_{abc} \right.$$
$$\left. + \frac{4}{3} \delta(N_f, 4) \mathcal{G}_{abcd} \bar{\sigma}_d \right] \sigma_a \sigma_b \sigma_c$$
$$- [4 \mathcal{H}_{abcd} \bar{\sigma}_d + 3 \delta(N_f, 3) \mathcal{G}_{abc}$$
$$- 4 \delta(N_f, 4) \mathcal{G}_{abcd} \bar{\sigma}_d] \pi_a \pi_b \sigma_c$$
$$- 2 [\mathcal{H}_{abcd} - \delta(N_f, 4) \mathcal{G}_{abcd}] \sigma_a \sigma_b \pi_c \pi_d$$
$$- \frac{1}{3} [\mathcal{F}_{abcd} + \delta(N_f, 4) \mathcal{G}_{abcd}]$$
$$\times (\sigma_a \sigma_b \sigma_c \sigma_d + \pi_a \pi_b \pi_c \pi_d) - U(\bar{\sigma}), \tag{22}$$

where $\delta(n, m) \equiv \delta_{nm}$ is the Kronecker delta and the fields σ_a and π_a are the fluctuations around the expectation values $\bar{\sigma}_a$. The latter are determined from the condition $dU(\bar{\sigma})/d\bar{\sigma}_a = 0$. The tree-level potential is

$$U(\bar{\sigma}) = \frac{m^2}{2} \bar{\sigma}_a^2 - [3 \delta(N_f, 2) \mathcal{G}_{ab} + \delta(N_f, 3) \mathcal{G}_{abc} \bar{\sigma}_c] \bar{\sigma}_a \bar{\sigma}_b$$
$$+ \frac{1}{3} [\mathcal{F}_{abcd} + \delta(N_f, 4) \mathcal{G}_{abcd}] \bar{\sigma}_a \bar{\sigma}_b \bar{\sigma}_c \bar{\sigma}_d - h_a \bar{\sigma}_a. \tag{23}$$

The coefficients $\mathcal{F}_{abcd}$, $\mathcal{G}_{ab}$, $\mathcal{G}_{abc}$, $\mathcal{G}_{abcd}$, and $\mathcal{H}_{abcd}$ are given by

$$\mathcal{F}_{abcd} = \frac{\lambda_1}{4} (\delta_{ab} \delta_{cd} + \delta_{ad} \delta_{bc} + \delta_{ac} \delta_{bd})$$
$$+ \frac{\lambda_2}{8} (d_{abn} d_{ncd} + d_{adn} d_{nbc} + d_{acn} d_{nbd}), \tag{24a}$$

$$\mathcal{G}_{ab} = \frac{c}{6} [\delta_{a0} \delta_{b0} - \delta_{a1} \delta_{b1} - \delta_{a2} \delta_{b2} - \delta_{a3} \delta_{b3}], \tag{24b}$$

$$\mathcal{G}_{abc} = \frac{c}{6} \left[d_{abc} - \frac{3}{2} (\delta_{a0} d_{0bc} + \delta_{b0} d_{a0c} + \delta_{c0} d_{ab0}) \right.$$
$$\left. + \frac{9}{2} d_{000} \delta_{a0} \delta_{b0} \delta_{c0} \right], \tag{24c}$$

$$\mathcal{G}_{abcd} = -\frac{c}{16} [\delta_{ab} \delta_{cd} + \delta_{ad} \delta_{bc} + \delta_{ac} \delta_{bd}$$
$$- (d_{abn} d_{ncd} + d_{adn} d_{nbc} + d_{acn} d_{nbd})$$
$$+ 16 \delta_{a0} \delta_{b0} \delta_{c0} \delta_{d0} - 4 (\delta_{a0} \delta_{b0} \delta_{cd} + \delta_{a0} \delta_{c0} \delta_{bd}$$
$$+ \delta_{a0} \delta_{d0} \delta_{bc} + \delta_{b0} \delta_{c0} \delta_{ad} + \delta_{b0} \delta_{d0} \delta_{ac}$$
$$+ \delta_{d0} \delta_{c0} \delta_{ab}) + \sqrt{8} (\delta_{a0} d_{bcd} + \delta_{b0} d_{cda} + \delta_{c0} d_{dab}$$
$$+ \delta_{d0} d_{abc})], \tag{24d}$$

$$\mathcal{H}_{abcd} = \frac{\lambda_1}{4} \delta_{ab} \delta_{cd} + \frac{\lambda_2}{8} (d_{abn} d_{ncd} + f_{acn} f_{nbd} + f_{bcn} f_{nad}). \tag{24e}$$

The tree-level masses, $[m_S^2]_{ab}$ and $[m_P^2]_{ab}$, are given by

$$[m_S^2(\bar{\sigma})]_{ab} = m^2 \delta_{ab} - 6 [\delta(N_f, 2) \mathcal{G}_{ab} + \delta(N_f, 3) \mathcal{G}_{abc} \bar{\sigma}_c]$$
$$+ 4 [\mathcal{F}_{abcd} + \delta(N_f, 4) \mathcal{G}_{abcd}] \bar{\sigma}_c \bar{\sigma}_d, \tag{25a}$$

$$[m_P^2(\bar{\sigma})]_{ab} = m^2 \delta_{ab} + 6 [\delta(N_f, 2) \mathcal{G}_{ab} + \delta(N_f, 3) \mathcal{G}_{abc} \bar{\sigma}_c]$$
$$+ 4 [\mathcal{H}_{abcd} - \delta(N_f, 4) \mathcal{G}_{abcd}] \bar{\sigma}_c \bar{\sigma}_d. \tag{25b}$$

In general, these mass matrices are not diagonal. Consequently, the fields (σ_a, π_a) in the standard basis of $U(N_f)$ generators are not mass eigenstates. Since the mass matrices are symmetric and real, diagonalization is achieved by an orthogonal transformation,

$$\tilde{\sigma}_i = O_{ia}^{(S)} \sigma_a, \tag{26a}$$

$$\tilde{\pi}_i = O_{ia}^{(P)} \pi_a, \tag{26b}$$

$$[\tilde{m}_{S,P}^2]_i = O_{ai}^{(S,P)} [m_{S,P}^2]_{ab} O_{bi}^{(S,P)}. \tag{26c}$$

The effective potential of the $U(N_f)_r \times U(N_f)_\ell$ linear sigma model in the CJT formalism reads

$$V[\bar{\sigma}, \bar{S}, \bar{P}] = U(\bar{\sigma}) + \frac{1}{2} \int_k \{ [\ln \bar{S}^{-1}(k)]_{aa} + [\ln \bar{P}^{-1}(k)]_{aa} \}$$

$$+ \frac{1}{2} \int_k [S_{ab}^{-1}(k;\bar{\sigma}) \bar{S}_{ba}(k) + P_{ab}^{-1}(k;\bar{\sigma}) \bar{P}_{ba}(k)$$

$$- 2 \delta_{ab} \delta_{ba}] + V_2[\bar{\sigma}, \bar{S}, \bar{P}]. \tag{27}$$

Here, $U(\bar{\sigma})$ is the tree-level potential of Eq. (23), and

$$S_{ab}^{-1}(k;\bar{\sigma}) = -k^2 \delta_{ab} + [m_S^2(\bar{\sigma})]_{ab}, \tag{28a}$$

$$P_{ab}^{-1}(k;\bar{\sigma}) = -k^2 \delta_{ab} + [m_P^2(\bar{\sigma})]_{ab}, \tag{28b}$$

are the tree-level propagators for scalar and pseudoscalar particles, with the respective mass matrices (25). The fluctuations σ_a and π_a around the expectation values $\bar{\sigma}_a$ no longer occur in the effective potential (27). Therefore, from now on we use the symbol σ_a for the expectation values for the scalar fields in the effective potential (27). These expectation values, and the full propagators for scalar, $\mathcal{S}(k)$, and pseudoscalar, $\mathcal{P}(k)$, particles are determined from the stationarity conditions

$$\left. \frac{\delta V[\bar{\sigma}, \bar{S}, \bar{P}]}{\delta \bar{\sigma}_a} \right|_{\bar{\sigma}=\sigma, \bar{S}=\mathcal{S}, \bar{P}=\mathcal{P}} = 0, \tag{29a}$$

$$\left. \frac{\delta V[\bar{\sigma}, \bar{S}, \bar{P}]}{\delta \bar{S}_{ab}} \right|_{\bar{\sigma}=\sigma, \bar{S}=\mathcal{S}, \bar{P}=\mathcal{P}} = 0,$$

$$\left. \frac{\delta V[\bar{\sigma}, \bar{S}, \bar{P}]}{\delta \bar{P}_{ab}} \right|_{\bar{\sigma}=\sigma, \bar{S}=\mathcal{S}, \bar{P}=\mathcal{P}} = 0. \tag{29b}$$

With Eq. (6b), the latter two equations can be written in the form

$$\mathcal{S}_{ab}^{-1}(k) = S_{ab}^{-1}(k;\bar{\sigma}) + \Sigma_{ab}(k), \tag{30a}$$

$$\mathcal{P}_{ab}^{-1}(k) = P_{ab}^{-1}(k;\bar{\sigma}) + \Pi_{ab}(k), \tag{30b}$$

where

$$\Sigma_{ab}(k) \equiv 2 \left. \frac{\delta V_2[\bar{\sigma}, \bar{S}, \bar{P}]}{\delta \bar{S}_{ba}(k)} \right|_{\bar{\sigma}=\sigma, \bar{S}=\mathcal{S}, \bar{P}=\mathcal{P}}, \tag{31a}$$

$$\Pi_{ab}(k) \equiv 2 \left. \frac{\delta V_2[\bar{\sigma}, \bar{S}, \bar{P}]}{\delta \bar{P}_{ba}(k)} \right|_{\bar{\sigma}=\sigma, \bar{S}=\mathcal{S}, \bar{P}=\mathcal{P}}, \tag{31b}$$

are the self-energies for the scalar and pseudoscalar particles. As in the case of the $O(N)$ model, we include only the two-loop diagrams of Fig. 1 in V_2. Then,

$$V_2[\bar{S}, \bar{P}] = [\mathcal{F}_{abcd} + \delta(N_f, 4)\mathcal{G}_{abcd}]$$

$$\times \left[\int_k \bar{S}_{ab}(k) \int_p \bar{S}_{cd}(p) + \int_k \bar{P}_{ab}(k) \int_p \bar{P}_{cd}(p) \right]$$

$$+ 2[\mathcal{H}_{abcd} - \delta(N_f, 4)\mathcal{G}_{abcd}] \int_k \bar{S}_{ab}(k) \int_p \bar{P}_{cd}(p). \tag{32}$$

Note that, in the Hartree approximation, V_2 is independent of $\bar{\sigma}_a$. The stationarity conditions for the condensates are

$$h_a = m^2 \sigma_a - [6 \delta(N_f, 2)\mathcal{G}_{ab} + 3 \delta(N_f, 3)\mathcal{G}_{abc} \sigma_c] \sigma_b$$

$$+ \frac{4}{3} [\mathcal{F}_{abcd} + \delta(N_f, 4)\mathcal{G}_{abcd}] \sigma_b \sigma_c \sigma_d$$

$$+ \{ -3 \delta(N_f, 3)\mathcal{G}_{abc} + 4[\mathcal{F}_{abcd} + \delta(N_f, 4)\mathcal{G}_{abcd}] \sigma_d \}$$

$$\times \int_k \mathcal{S}_{cb}(k) + \{ 3 \delta(N_f, 3)\mathcal{G}_{abc} + 4[\mathcal{H}_{bcad}$$

$$- \delta(N_f, 4)\mathcal{G}_{abcd}] \sigma_d \} \int_k \mathcal{P}_{cb}(k). \tag{33}$$

In the Hartree approximation, the self-energies (6b) are independent of momentum, and the Schwinger-Dyson equations (30a) for the full propagators assume the simple form

$$\mathcal{S}_{ab}^{-1}(k) = -k^2 \delta_{ab} + [M_S^2]_{ab}, \tag{34}$$

$$\mathcal{P}_{ab}^{-1}(k) = -k^2 \delta_{ab} + [M_P^2]_{ab}. \tag{35}$$

The scalar and pseudoscalar mass matrices are given by

$$[M_S^2]_{ab} = [m_S^2(\sigma)]_{ab} + 4[\mathcal{F}_{abcd} + \delta(N_f, 4)\mathcal{G}_{abcd}] \int_q \mathcal{S}_{cd}(q)$$

$$+ 4[\mathcal{H}_{abcd} - \delta(N_f, 4)\mathcal{G}_{abcd}] \int_q \mathcal{P}_{cd}(q), \tag{36a}$$

$$[M_P^2]_{ab} = [m_P^2(\sigma)]_{ab} + 4[\mathcal{F}_{abcd} + \delta(N_f, 4)\mathcal{G}_{abcd}] \int_q \mathcal{P}_{cd}(q)$$

$$+ 4[\mathcal{H}_{abcd} - \delta(N_f, 4)\mathcal{G}_{abcd}] \int_q \mathcal{S}_{cd}(q). \tag{36b}$$

In the Hartree approximation, all particles are stable quasiparticles, i.e., the imaginary parts of the self-energies vanish. Therefore, the inverse propagators (34) and (35) are real valued. They are also symmetric in the standard basis of $U(N_f)$ generators and thus diagonalizable via an orthogonal transformation. This transformation is given by Eq. (26c), with the obvious replacements

$$[m^2_{S,P}]_{ab} \to [M^2_{S,P}]_{ab}, \quad [\tilde{m}^2_{S,P}]_i \to [\tilde{M}^2_{S,P}]_i. \quad (37)$$

The propagator matrices are diagonalized by the same orthogonal transformation as their inverse. The tadpole integrals in Eqs. (33) and (36) are therefore computed as

$$\int_q \mathcal{S}_{bc}(q) = O^{(S)}_{bi} \int_q \tilde{\mathcal{S}}_i(q) O^{(S)}_{ci},$$

$$\int_q \mathcal{P}_{bc}(q) = O^{(P)}_{bi} \int_q \tilde{\mathcal{P}}_i(q) O^{(P)}_{ci}. \quad (38)$$

After this rotation, only tadpole integrals over propagators with a single index have to be computed. This will be discussed in the next section.

D. Explicit calculation of loop integrals and the effective potential

In principle, the calculation of the tadpole integrals $\int_q \tilde{\mathcal{S}}_i(q)$, $\int_q \mathcal{S}(q)$ and $\int_q \tilde{\mathcal{P}}_i(q)$, $\int_q \mathcal{P}(q)$ requires renormalization. Renormalization of many-body approximation schemes is nontrivial, but does not change the results qualitatively [9,10]. We therefore simply omit the vacuum contributions to the loop integrals,

$$\int_q \tilde{\mathcal{S}}_i(q) = \int \frac{d^3\mathbf{q}}{(2\pi)^3} \frac{1}{\epsilon_{\mathbf{q}}[(\tilde{M}^2_S)_i]} \left(\exp\left\{ \frac{\epsilon_{\mathbf{q}}[(\tilde{M}^2_S)_i]}{T} \right\} - 1 \right)^{-1},$$
$$(39a)$$

$$\int_q \tilde{\mathcal{P}}_i(q) = \int \frac{d^3\mathbf{q}}{(2\pi)^3} \frac{1}{\epsilon_{\mathbf{q}}[(\tilde{M}^2_P)_i]} \left(\exp\left\{ \frac{\epsilon_{\mathbf{q}}[(\tilde{M}^2_P)_i]}{T} \right\} - 1 \right)^{-1},$$
$$(39b)$$

$$\int_q \mathcal{S}(q) = \int \frac{d^3\mathbf{q}}{(2\pi)^3} \frac{1}{\epsilon_{\mathbf{q}}[M^2_\sigma]} \left(\exp\left\{ \frac{\epsilon_{\mathbf{q}}[M^2_\sigma]}{T} \right\} - 1 \right)^{-1},$$
$$(39c)$$

$$\int_q \mathcal{P}(q) = \int \frac{d^3\mathbf{q}}{(2\pi)^3} \frac{1}{\epsilon_{\mathbf{q}}[M^2_\pi]} \left(\exp\left\{ \frac{\epsilon_{\mathbf{q}}[M^2_\pi]}{T} \right\} - 1 \right)^{-1}.$$
$$(39d)$$

Here, $\epsilon_{\mathbf{q}}[M^2] = \sqrt{\mathbf{q}^2 + M^2}$ is the relativistic energy of a quasiparticle with mass M and momentum $\mathbf{q}$.

Now we compute the standard effective potential $V(\bar{\sigma})$ $\equiv V[\bar{\sigma}, \hat{S}(\bar{\sigma}), \hat{P}(\bar{\sigma})]$ from Eq. (10). Since V_2 has the general structure

$$V_2[\bar{S},\bar{P}] = c_s \left[\int_k \bar{S}(k) \right]^2 + c_p \left[\int_k \bar{P}(k) \right]^2$$

$$+ c_{sp} \left[\int_k \bar{S}(k) \right] \left[\int_p \bar{P}(p) \right], \quad (40)$$

cf. Eqs. (15) and (27), the self-energies (31) assume the form

$$\hat{\Sigma}(k;\bar{\sigma}) = 2 \frac{\delta V_2[\bar{\sigma},\bar{S},\bar{P}]}{\delta \bar{S}(k)} \Bigg|_{\bar{\sigma}=\sigma, \bar{S}=\hat{S}, \bar{P}=\hat{P}}$$

$$= 4c_s \int_q \hat{S}(q;\bar{\sigma}) + 2c_{sp} \int_q \hat{P}(q;\bar{\sigma}), \quad (41a)$$

$$\hat{\Pi}(k;\bar{\sigma}) = 2 \frac{\delta V_2[\bar{\sigma},\bar{S},\bar{P}]}{\delta \bar{P}(k)} \Bigg|_{\bar{\sigma}=\sigma, \bar{S}=\hat{S}, \bar{P}=\hat{P}}$$

$$= 4c_p \int_q \hat{P}(q;\bar{\sigma}) + 2c_{sp} \int_q \hat{S}(q;\bar{\sigma}). \quad (41b)$$

With these expressions one derives the identity

$$-\frac{1}{2} \int_k \hat{\Sigma}(k;\bar{\sigma}) \hat{S}(k;\bar{\sigma}) - \frac{1}{2} \int_k \hat{\Pi}(k;\bar{\sigma}) \hat{P}(k;\bar{\sigma})$$

$$\equiv -2 V_2[\hat{S}(\bar{\sigma}), \hat{P}(\bar{\sigma})]. \quad (42)$$

This considerably simplifies the expressions for the standard effective potential. For the $O(N)$ model we obtain

$$V(\bar{\sigma}) = U(\bar{\sigma}) + \frac{1}{2} \int_k \ln \hat{S}^{-1}(k;\bar{\sigma}) + \frac{N-1}{2} \int_k \ln \hat{P}^{-1}(k;\bar{\sigma})$$

$$- V_2[\hat{S}(\bar{\sigma}), \hat{P}(\bar{\sigma})], \quad (43a)$$

while for the $U(N_f)_r \times U(N_f)_\ell$ model we have

$$V(\bar{\sigma}) = U(\bar{\sigma}) + \frac{1}{2} \sum_{i=0}^{N_f^2-1} \int_k \ln \hat{\tilde{S}}_i^{-1}(k;\bar{\sigma})$$

$$+ \frac{1}{2} \sum_{i=0}^{N_f^2-1} \int_k \ln \hat{\tilde{P}}_i^{-1}(k;\bar{\sigma}) - V_2[\hat{S}(\bar{\sigma}), \hat{P}(\bar{\sigma})]. \quad (43b)$$

The momentum integrals in Eqs. (43a) and (43b) require renormalization, too. As above, we simply omit the vacuum contribution, which leads to the following integrals [8]:

$$\int_k \ln \hat{\tilde{S}}_i^{-1}(k;\bar{\sigma}) = T \int \frac{d^3\mathbf{k}}{(2\pi)^3} \ln\left(1 - \exp\left\{ -\frac{\epsilon_{\mathbf{k}}[(\hat{\tilde{M}}^2_S)_i]}{T} \right\} \right),$$
$$(44a)$$

$$\int_k \ln \hat{\tilde{P}}_i^{-1}(k;\bar{\sigma}) = T \int \frac{d^3\mathbf{k}}{(2\pi)^3} \ln\left(1 - \exp\left\{ -\frac{\epsilon_{\mathbf{k}}[(\hat{\tilde{M}}^2_P)_i]}{T} \right\} \right),$$
$$(44b)$$

$$\int_k \ln \hat{S}^{-1}(k;\bar{\sigma}) = T \int \frac{d^3\mathbf{k}}{(2\pi)^3} \ln\left(1 - \exp\left\{ -\frac{\epsilon_{\mathbf{k}}[\hat{M}^2_\sigma]}{T} \right\} \right),$$
$$(44c)$$

$$\int_k \ln \hat{\mathcal{P}}^{-1}(k;\bar{\sigma}) = T \int \frac{d^3\mathbf{k}}{(2\pi)^3} \ln\left(1 - \exp\left\{-\frac{\epsilon_\mathbf{k}[\hat{M}_\pi^2]}{T}\right\}\right).$$

(44d)

In these equations, the tilde denotes quantities which are diagonalized according to Eqs. (26c) and (38), respectively. A hat denotes propagators computed according to Eq. (9a). Masses with a hat are the mass terms appearing in these propagators.

III. PATTERNS OF SYMMETRY BREAKING AND VACUUM PROPERTIES

In this section we discuss the patterns of symmetry breaking in the vacuum and determine the coupling constants of the models from the vacuum properties of the mesons.

A. Patterns of symmetry breaking

For the $O(N)$ model (with $N=4$) we study two different patterns of symmetry breaking (cf. Table I):

(1) $H=0$. For $\mu^2<0$ the $O(N)$ symmetry is spontaneously broken to $O(N-1)$, giving rise to a non-vanishing expectation value for the σ field and $N-1$ Goldstone bosons.

(2) $H\neq0$. The term $-H\bar{\sigma}$ in Eq. (14) corresponds to non-zero quark masses in the QCD Lagrangian. It breaks the $O(N)$ symmetry explicitly to $O(N-1)$. The $N-1$ Goldstone bosons become pseudo-Goldstone bosons.

For the $U(N_f)_r \times U(N_f)_\ell$ models with $N_f=2$ and 3 we study the following patterns of symmetry breaking (cf. Table I).

(1) $h_a=0, c=0$. For $m^2<0$ the global $SU(N_f)_V \times U(N_f)_A$ symmetry is broken to $SU(N_f)_V$, and Φ develops a non-vanishing vacuum expectation value, $\langle\Phi\rangle = T_0\bar{\sigma}_0$. By the Vafa-Witten theorem [23], only the axial symmetries can be spontaneously broken, while the vector symmetries stay intact. In order to retain an $SU(N_f)_V$ symmetry, only the term proportional to T_0 survives in the sum over a in Eq. (21) for the vacuum expectation value $\langle\Phi\rangle$. Spontaneously breaking $U(N_f)_A$ leads to N_f^2 Goldstone bosons which form a pseudoscalar, N_f^2 dimensional multiplet. This case is referred to as the chiral limit without $U(1)_A$ anomaly.

(2) $h_a=0, c\neq0$. The symmetry is $SU(N_f)_V \times SU(N_f)_A$. A non-vanishing $\langle\Phi\rangle$ spontaneously breaks the symmetry to $SU(N_f)_V$, with the appearance of N_f^2-1 Goldstone bosons which form a pseudoscalar, N_f^2-1 dimensional multiplet. The N_f^2th pseudoscalar meson is no longer massless, because the $U(1)_A$ symmetry is already explicitly broken. This case is referred to as the chiral limit with $U(1)_A$ anomaly.

(3) $h_a\neq0, c=0$. In QCD this corresponds to non-vanishing quark masses, but a vanishing $U(1)_A$ anomaly. Since $\langle\Phi\rangle$ must carry the quantum numbers of the vacuum, only the fields $\bar{\sigma}_a$ corresponding to the diagonal generators of $U(N_f)$ can be nonzero. The same holds for the external fields h_a which generate a non-vanishing expectation value by explicitly breaking the $U(N_f)_A$ symmetry. For $N_f=2$

these are h_0 and h_3, for $N_f=3$ there is an additional field, h_8. Because the masses of the up and down quarks are approximately equal, $m_u\simeq m_d$, we restrict our study to $h_0\neq0$ and $h_3=0$ for all cases considered. Since the strange quark mass m_s is larger than $m_u\simeq m_d$, $h_8\neq0$. In this case the $SU(N_f)_V \times U(N_f)_A$ symmetry is explicitly broken to $SU(2)_V$. The latter symmetry remains intact because $h_3=0$. This case is referred to as the case of explicit chiral symmetry breaking without $U(1)_A$ anomaly.

(4) $h_a\neq, c\neq0$. A $U(1)_A$ subgroup of the $U(N_f)_A$ symmetry is explicitly broken by instantons. As explained above we restrict ourselves to $h_3=0$. This case is referred to as the case of explicit chiral symmetry breaking with $U(1)_A$ anomaly.

For $N_f=4$, we only study the last case, i.e., explicit chiral symmetry breaking with the $U(1)_A$ anomaly. To break the $U(4)_A$ symmetry explicitly, in addition to $h_0\neq0$ and $h_8 \neq0$, we have to introduce a nonzero value for the field h_{15} corresponding to the fourth diagonal generator of $U(4)$. Since the charm quark mass is much larger than the light up and down quark masses and the strange quark mass, h_{15} is also much larger than either h_0 or h_8, cf. Table V. Therefore, it does not make too much sense to study the rather unrealistic first two cases of vanishing quark masses. We therefore restrict our considerations to the physical case of explicit chiral symmetry breaking with the $U(1)_A$ anomaly.

B. Condensates and masses in the vacuum

In this section we determine the parameters of the different models from the vacuum values of the condensates and the meson masses for the various symmetry breaking patterns discussed in Sec. III A. For the $O(4)$, the $U(3)_r \times U(3)_\ell$, and the $U(4)_r \times U(4)_\ell$ linear sigma model, we simply follow Refs. [9,10,22], respectively. Since it has not been done previously, fitting the parameters of the $U(2)_r \times U(2)_\ell$ model is discussed in more detail.

For the $O(4)$ model, we have three parameters, H, λ, and μ^2, which are adjusted to reproduce the vacuum values for the pion decay constant, f_π, the pion mass, m_π, and the σ mass, m_σ. For reasons explained below, for the latter we choose $m_\sigma=400$ MeV, instead of 600 MeV as in Ref. [10]. The values for the parameters in the chiral limit and with explicit symmetry breaking are listed in Table II.

In the $U(2)_r \times U(2)_\ell$ model, for all symmetry breaking patterns studied here, there is an (approximate) $SU(2)_V$ symmetry due to the (approximate) equality of the up and down quark masses. Consequently, for all cases the vacuum expectation value is $\langle\Phi\rangle = T_0\bar{\sigma}_0$. At zero temperature, the equation for the condensate σ_0 reads, cf. Eq. (33),

$$h_0 = \sigma_0\left[m^2 - c + \left(\lambda_1 + \frac{\lambda_2}{2}\right)\sigma_0^2\right].$$

(45)

The PCAC (partial conservation of axial vector current) relations determine the value of the condensate from the pseudoscalar meson decay constants,

$$f_a = d_{aa0}\sigma_0.$$

(46)

TABLE II. The masses and decay constants at vanishing temperature and the corresponding parameter sets for the $O(4)$ linear sigma model for the two symmetry breaking patterns studied here.

	Masses and decay constants	Parameter set
Explicit chiral symmetry breaking	$f_\pi = 92.4$ MeV $m_\sigma = 400$ MeV $m_\pi = 139.5$ MeV	$H = (121.60 \text{ MeV})^3$ $\lambda = 8.230$ $\mu^2 = -(225.41 \text{ MeV})^2$
Chiral limit	$f_\pi = 90$ MeV $m_\sigma = 400$ MeV $m_\pi = 0$ MeV	$H = 0$ $\lambda = 9.877$ $\mu^2 = -(282.84 \text{ MeV})^2$

Since $d_{aa0} = 1$, all meson decay constants are identical, and we obtain $\sigma_0 \equiv f_\pi$. The scalar mass matrix is diagonal, with the elements

$$m_\sigma^2 \equiv [m_S^2(\sigma_0)]_{00} = m^2 - c + 3\left(\lambda_1 + \frac{\lambda_2}{2}\right)\sigma_0^2, \quad (47a)$$

$$m_{a_0}^2 \equiv [m_S^2(\sigma_0)]_{11}$$

$$= [m_S^2(\sigma_0)]_{22}$$

$$= [m_S^2(\sigma_0)]_{33}$$

$$= m^2 + c + \left(\lambda_1 + \frac{3\lambda_2}{2}\right)\sigma_0^2. \quad (47b)$$

The pseudoscalar mass matrix is also diagonal, with the elements

$$m_\eta^2 \equiv [m_P^2(\sigma_0)]_{00} = m^2 + c + \left(\lambda_1 + \frac{\lambda_2}{2}\right)\sigma_0^2, \quad (48a)$$

$$m_\pi^2 \equiv [m_P^2(\sigma_0)]_{11}$$

$$= [m_P^2(\sigma_0)]_{22}$$

$$= [m_P^2(\sigma_0)]_{33}$$

$$= m^2 - c + \left(\lambda_1 + \frac{\lambda_2}{2}\right)\sigma_0^2. \quad (48b)$$

Without the $U(1)_A$ anomaly, $c = 0$, the pions and the η meson become degenerate in mass. In the chiral limit, one then has four (instead of three) Goldstone bosons. With the $U(1)_A$

TABLE III. The masses and decay constants at vanishing temperature and the corresponding parameter sets for the $U(2)_r \times U(2)_\ell$ model for the four symmetry breaking patterns studied here.

	Masses and decay constants	Parameter set
Explicit chiral symmetry breaking with $U(1)_A$ anomaly	$f_\pi = 92.4$ MeV $m_\sigma = 400$ MeV $m_{a_0} = 984.7$ MeV $m_\pi = 139.5$ MeV $m_\eta = 547$ MeV	$h_0 = (121.60 \text{ MeV})^3$ $\lambda_1 = -31.03$ $\lambda_2 = 78.52$ $m^2 = (298.44 \text{ MeV})^2$ $c = (374.00 \text{ MeV})^2$
Explicit chiral symmetry breaking without $U(1)_A$ anomaly	$f_\pi = 92.4$ MeV $m_\sigma = 400$ MeV $m_{a_0} = 984.7$ MeV $m_\pi = m_\eta = 139.5$ MeV	$h_0 = (121.60 \text{ MeV})^3$ $\lambda_1 = -47.41$ $\lambda_2 = 111.29$ $m^2 = -(225.41 \text{ MeV})^2$ $c = 0$
Chiral limit with $U(1)_A$ anomaly	$f_\pi = 90$ MeV $m_\sigma = 400$ MeV $m_{a_0} = 984.7$ MeV $m_\pi = 0$ $m_\eta = 547$ MeV	$h_0 = 0$ $\lambda_1 = -31.51$ $\lambda_2 = 82.77$ $m^2 = (263.83 \text{ MeV})^2$ $c = (386.79 \text{ MeV})^2$
Chiral limit without $U(1)_A$ anomaly	$f_\pi = 90$ MeV $m_\sigma = 400$ MeV $m_{a_0} = 984.7$ MeV $m_\pi = m_\eta = 0$	$h_0 = c = 0$ $\lambda_1 = -49.98$ $\lambda_2 = 119.71$ $m^2 = -(282.84 \text{ MeV})^2$

TABLE IV. The masses and decay constants at vanishing temperature and the corresponding parameter sets for the $U(3)_r \times U(3)_\ell$ model for the four symmetry breaking patterns studied here. The masses in boldfaced letters are predicted; the other masses and decay constants are used to calculate the parameter set.

	Masses and decay constants	Parameter set
Explicit chiral symmetry beaking with $U(1)_A$ anomaly	$f_\pi = 92.4$ MeV $f_K = 113$ MeV $m_\sigma = 400$ MeV $\mathbf{m}_{a_0} = \mathbf{1024.6}$ MeV $\mathbf{m}_\kappa = \mathbf{1116.2}$ MeV $\mathbf{m}_{f_0} = \mathbf{1188.7}$ MeV $m_\pi = 139.5$ MeV $m_K = 493$ MeV $\mathbf{m}_\eta = \mathbf{536.5}$ MeV $\mathbf{m}_{\eta'} = \mathbf{963.9}$ MeV	$h_0 = (285.04 \text{ MeV})^3$ $h_8 = -(309.46 \text{ MeV})^3$ $\lambda_1 = -5.38$ $\lambda_2 = 45.08$ $m^2 = (493.69 \text{ MeV})^2$ $c = 4831.25$ MeV
Explicit chiral symmetry breaking without $U(1)_A$ anomaly	$f_\pi = 92.4$ MeV $f_K = 113$ MeV $m_\sigma = 400$ MeV $\mathbf{m}_{a_0} = \mathbf{844.4}$ MeV $\mathbf{m}_\kappa = \mathbf{1116.2}$ MeV $\mathbf{m}_{f_0} = \mathbf{1248.3}$ MeV $m_\pi = m_{\eta'} = 139.5$ MeV $m_K = 493$ MeV $\mathbf{m}_\eta = \mathbf{630.6}$ MeV	$h_0 = (285.04 \text{ MeV})^3$ $h_8 = -(309.46 \text{ MeV})^3$ $\lambda_1 = -24.13$ $\lambda_2 = 81.24$ $m^2 = (306.50 \text{ MeV})^2$ $c = 0$
Chiral limit with $U(1)_A$ anomaly	$f_\pi = f_K = 90$ MeV $m_\sigma = 400$ MeV $m_{a_0} = m_\kappa = m_{f_0} = 1225.8$ MeV $m_\pi = m_K = m_\eta = 0$ $m_{\eta'} = 958$ MeV	$h_0 = h_8 = 0$ $\lambda_1 = -17.48$ $\lambda_2 = 109.97$ $m^2 = (270.11 \text{ MeV})^2$ $c = 6798.25$ MeV
Chiral limit without $U(1)_A$ anomaly	$f_\pi = f_K = 90$ MeV $m_\sigma = 400$ MeV $m_{a_0} = m_\kappa = m_{f_0} = 1225.8$ MeV $m_\pi = m_K = m_\eta = m_{\eta'} = 0$	$h_0 = h_8 = c = 0$ $\lambda_1 = -55.25$ $\lambda_2 = 185.50$ $m^2 = -(282.84 \text{ MeV})^2$

anomaly, c is positive, cf. Table III, and the η meson becomes heavier than the pion. At zero temperature, the (squared) mass difference between the η and the pion is determined by the parameter c characterizing the strength of the $U(1)_A$ anomaly, $m_\eta^2 - m_\pi^2 = 2c$. Simultaneously, also the mass difference between the a_0 and the σ meson is determined by this parameter, $m_{a_0}^2 - m_\sigma^2 = 2c - 2\lambda_1 \sigma_0^2$. (As $\lambda_1 < 0$, cf. Table III, the second term always increases the mass difference.)

The limit $c \to \infty$ corresponds to maximum explicit $U(1)_A$ symmetry breaking. In this limit, for realistic values of the σ meson and the pion mass (i.e., $m^2 - c = \text{const}$), the η and a_0 mesons become infinitely heavy and are thus removed from the spectrum of physical excitations. In this limit, the $U(2)_r \times U(2)_\ell$ is identical to the $O(4)$ model, where the a_0 and η meson are absent from the beginning.

With Eqs. (45), (47), and (48), we can determine the parameters of the model from the pion decay constant and the meson masses in the vacuum,

$$\sigma_0 = f_\pi, \quad \lambda_1 = \frac{m_\sigma^2 - m_\pi^2 - m_{a_0}^2 + m_\eta^2}{2 f_\pi^2}, \quad \lambda_2 = \frac{m_{a_0}^2 - m_\eta^2}{f_\pi^2},$$

$$m^2 = m_\pi^2 + \frac{m_\eta^2 - m_\sigma^2}{2}, \quad c = \frac{m_\eta^2 - m_\pi^2}{2}, \quad h_0 = f_\pi m_\pi^2. \quad (49)$$

With the $U(1)_A$ anomaly, there are five parameters, h_0, λ_1, λ_2, m^2, and c, which can be unambiguously determined from the five quantities f_π, m_σ, m_{a_0}, m_η, and m_π. Without the $U(1)_A$ anomaly, $c = 0$, and $m_\eta = m_\pi$. In this case, there are only four parameters and four quantities from which the values of the parameters can be fixed. The values for the parameters are listed in Table III.

For the $U(3)_r \times U(3)_\ell$ model, we follow Ref. [9] in fitting the parameters of the model to vacuum quantities. Our parameters differ from the ones given in Ref. [9], since we use $m_\sigma = 400$ MeV, and not 600 MeV. In the chiral limit, the number of parameters equals the number of vacuum quanti-

TABLE V. The masses and decay constants at vanishing temperature and the corresponding parameter sets for the $U(4)_r \times U(4)_\ell$ model for the case of explicit chiral symmetry breaking with $U(1)_A$ anomaly. The masses written in boldfaced letters are predicted; the other masses and decay constants are used to calculate the parameter set.

	Masses and decay constants	Parameter set
Explicit chiral	$f_\pi = 92.4$ MeV	$h_0 = (917.24 \text{ MeV})^3$
symmetry breaking	$f_K = 113$ MeV	$h_8 = -(309.46 \text{ MeV})^3$
with $U(1)_A$	$\mathbf{m}_\sigma = \mathbf{400.6}$ MeV	$h_{15} = -(1088.67 \text{ MeV})^3$
anomaly	$\mathbf{m}_{a_0} = \mathbf{1052.6}$ MeV	$\lambda_1 = -0.12$
	$\mathbf{m}_\kappa = \mathbf{1116.2}$ MeV	$\lambda_2 = 4.85$
	$\mathbf{m}_{f_0} = \mathbf{1178.6}$ MeV	$m^2 = (345.78 \text{ MeV})^2$
	$\mathbf{m}_{D_0} = \mathbf{2370.0}$ MeV	$c = -1.50$
	$\mathbf{m}_{D_{s0}} = \mathbf{2480.1}$ MeV	
	$\mathbf{m}_{\chi_{c0}} = \mathbf{3565.6}$ MeV	
	$m_\pi = 139.5$ MeV	
	$m_K = 493$ MeV	
	$\mathbf{m}_\eta = \mathbf{542.5}$ MeV	
	$\mathbf{m}_{\eta'} = \mathbf{1028}$ MeV	
	$\mathbf{m}_D = \mathbf{1944.1}$ MeV	
	$\mathbf{m}_{D_s} = \mathbf{1899.1}$ MeV	
	$\mathbf{m}_{\eta_c} = \mathbf{2129.8}$ MeV	

ties, and one can again obtain a unique mapping between these sets of quantities. With explicit chiral symmetry breaking, however, there are fewer parameters than vacuum quantities. Consequently, some meson masses are predicted rather than used as fit parameters. The values for the parameters and the meson masses are given in Table IV. The vacuum quantities predicted by the fit are given in bold-faced letters.

For the $U(4)_r \times U(4)_\ell$ model we adjust the parameters to obtain reasonable agreement between the vacuum masses [24] and the masses computed at tree level, and not the masses computed to one-loop order as in Ref. [22]. As for the $U(3)_r \times U(3)_\ell$ case, the number of parameters is smaller than the number of meson masses, such that some meson masses cannot be fitted independently, but are predicted within this approach. We found that small values for the σ meson, $m_\sigma \sim 400$ MeV, are favored, otherwise the mass spectrum of the charmed mesons deviates too much from the one in nature. This is the reason why we choose a σ meson mass $m_\sigma = 400$ MeV also in the other cases discussed above. The values for the parameters and vacuum quantities are listed in Table V.

IV. RESULTS

In this section we discuss the numerical results at nonzero temperature for the cases listed in Table I.

A. Explicit chiral symmetry breaking with $U(1)_A$ anomaly

In Fig. 2 we show the masses of the mesons as a function of temperature for explicit chiral symmetry breaking, including the $U(1)_A$ anomaly. This is the case where chiral symmetry breaking results in the smallest residual symmetry group, $SU(N_f)_V \times U(N_f)_A \to SU(2)_V$.

In Fig. 2(a) the masses of the σ meson and the pions are shown for all models. The σ meson and the pion become degenerate in mass in the chirally restored phase. Comparing the σ meson and pion masses in the $O(4)$ model with those in the $U(2)_r \times U(2)_\ell$ model, the difference is almost negligible up to temperatures of 150 MeV. In the chirally restored phase, the masses behave linearly with temperature, but grow faster in the $U(2)_r \times U(2)_\ell$ model than in the $O(4)$ model. The reason is that there are twice as many fields in the former model than in the latter, which results in twice as many tadpole-like contributions in the equations for the in-medium masses. These come with a positive sign and thus increase the masses.

Comparing the results of the $U(3)_r \times U(3)_\ell$ model with those of the $U(2)_r \times U(2)_\ell$ model, one observes differences already at a temperature of about 100 MeV. Furthermore, the masses become even larger in the chirally restored phase. The reason for this behavior is the strange degrees of freedom in the $N_f = 3$ case which lead to additional tadpole-like terms in the self-energies. As above, they lead to an increase of the in-medium masses.

Finally, one observes that virtually nothing changes in the temperature range of interest when including the charm degrees of freedom in the framework of the $U(4)_r \times U(4)_\ell$ model. The reason is that the charm quark is large compared to the temperature, $m_c \gg T$, and the contributions from charmed particles to the equations for the in-medium masses are suppressed. For two reasons, this is a non-trivial result. First, the equations for the in-medium masses are structurally different for the $U(4)_r \times U(4)_\ell$ model as compared to the $U(3)_r \times U(3)_\ell$ model, cf. Eqs. (25) and (36). Second, although the tadpole terms (39) are strongly suppressed for particles with masses much larger than the temperature, Eqs. (33) and (36) form a *nonlinear* system of coupled equations,
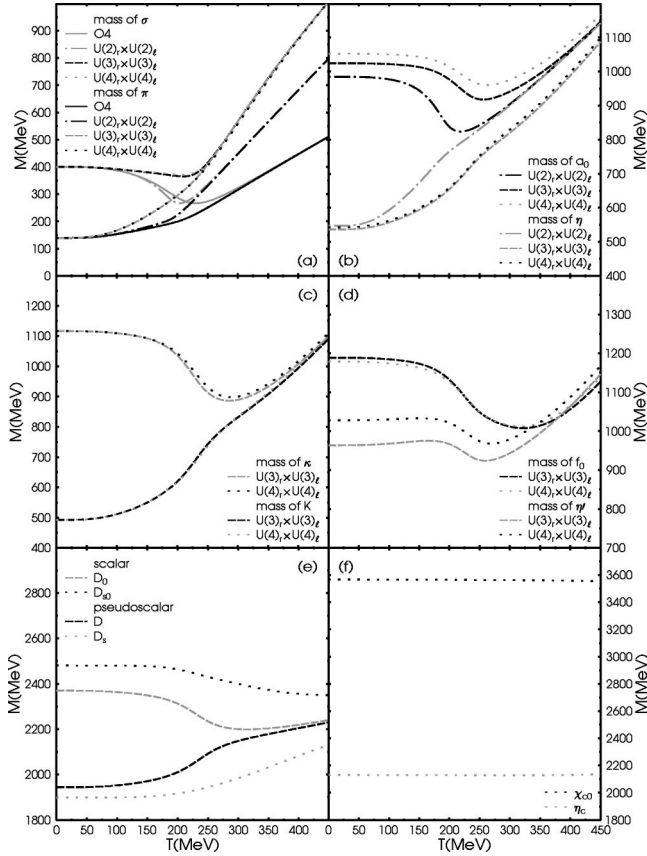
FIG. 2. The meson masses as a function of temperature for the different models studied here for the case with the $U(1)_A$ anomaly and explicit chiral symmetry breaking.
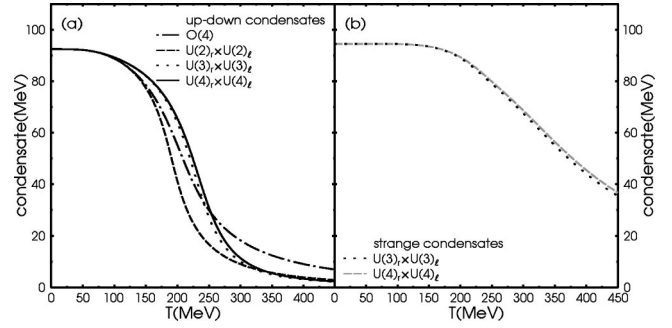

FIG. 3. (a) The up-down quark condensate and (b) the strange quark condensate as functions of temperature for the different models in the case with $U(1)_A$ anomaly and explicitly broken chiral symmetry.

i.e., small perturbations could lead to large quantitative changes in the solution.

In Fig. 2(b) the masses of the a_0 and the η mesons are shown as functions of temperature. Qualitatively, the behavior of these masses is the same in all models. The a_0 meson mass is constant up to temperatures of 150–200 MeV. It then decreases, before increasing again above temperatures of 200–250 MeV. The η meson mass is constant up to $T \simeq 50$ MeV, and then monotonously increases with temperature. At large temperatures, a_0 and η become degenerate in mass, indicating restoration of chiral symmetry. In the $U(2)_r \times U(2)_\ell$ model, this happens somewhat earlier, at about 250 MeV, than in the other two cases.

In the $U(2)_r \times U(2)_\ell$ model, the a_0 and η meson masses are used to determine the parameters of the model. Thus, at zero temperature, the masses coincide with their correct vacuum values. In the $U(3)_r \times U(3)_\ell$ model, the predicted η mass deviates only by 2% from its vacuum value. The a_0 mass is also rather close to the correct value; the predicted mass is about 4% too large. In the $U(4)_r \times U(4)_\ell$, the η mass is reproduced with excellent accuracy (the deviation is less than 1%), while the a_0 mass is within 7% of its vacuum value.

In Fig. 2(c) the κ meson [now referred to as $K_0^*(1430)$ [24]] and kaon masses are shown as a function of temperature. The results for the $U(3)_r \times U(3)_\ell$ and $U(4)_r \times U(4)_\ell$

model are almost identical. The κ meson and kaon become degenerate in mass at temperatures of the order of 400 MeV. In both models, the vacuum kaon mass is used as input, while the κ mass is predicted. The deviation to the vacuum value in nature is about 21%.

Figure 2(d) shows the masses of the f_0 and the η' meson as a function of temperature. These mesons also become degenerate in mass at temperatures of the order of 400 MeV. In the $U(3)_r \times U(3)_\ell$ model, the predicted η' mass is rather close to its value in nature; the deviation is 0.6%. In the $U(4)_r \times U(4)_\ell$ model, the η' mass deviates from its correct vacuum value by about 7%. The f_0 mass is predicted in both models. If we identify this state with the $f_0(1370)$, these predicted masses deviate by 14% from their correct values.

The masses of the D_{s0}, D_0, D_s, and D mesons are shown in Fig. 2(e). The masses of the pseudoscalar mesons are known but the scalar mesons and their masses have not yet been experimentally identified. It is somewhat peculiar that the charmed, strange D_s meson is lighter than the charmed, non-strange D meson. This is an artifact of the particular set of coupling constants chosen here. For a different choice, this unphysical ordering of the masses can be reversed. Then, however, the masses of the other mesons deviate by an unacceptably large extent from their physical values. Temperature has virtually no effect on the heavy charmed mesons: their mass changes at most by 10%, even in the chirally restored phase. Because of the non-linear nature of the coupled system of Eqs. (33) and (36), this is a non-trivial result, although not completely unexpected: we expect significant changes of the meson masses only when the temperature becomes of the order of the mass. For the charmed mesons with masses of the order of 2 GeV, this is never the case in the temperature range of interest.

Finally, in Fig. 2(f) we show the masses of the χ_{c0} and η_c meson. Their large masses do not change at all for temperatures below 450 MeV. The vacuum values for both meson masses are predicted. While the mass for the χ_{c0} is within 5% of its correct value, the deviation for the η_c is somewhat larger ($\simeq 30\%$).

To summarize, the masses of the scalar mesons remain approximately constant up to temperatures around 150 MeV, and then slightly decrease before they become degenerate with the masses of the pseudoscalar mesons. On the other
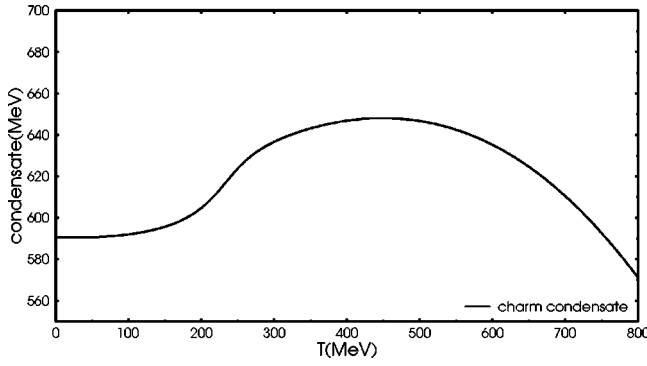
FIG. 4. The charm quark condensate as a function of temperature.

hand, with the exception of the η' mass, the pseudoscalar masses in general increase monotonously with temperature.

In Fig. 3(a) the up-down quark condensate and in 3(b) the strange quark condensate are shown as functions of temperature. In the $O(4)$ model and in the $U(2)_r \times U(2)_\ell$ model the up-down quark condensate $\varphi_{\text{up-down}}$ can be directly identified with the vacuum expectation value of the σ field, $\varphi_{\text{up-down}} \equiv \sigma_0$. On the other hand, in the $U(3)_r \times U(3)_\ell$ model [9],

$$\varphi_{\text{up-down}} = \sqrt{\frac{2}{3}}\sigma_0 + \frac{1}{\sqrt{3}}\sigma_8, \qquad (50a)$$

$$\varphi_{\text{strange}} = \frac{1}{\sqrt{3}}\sigma_0 - \sqrt{\frac{2}{3}}\sigma_8, \qquad (50b)$$

and in the $U(4)_r \times U(4)_\ell$ model the condensates are given by

$$\varphi_{\text{up-down}} = \frac{1}{\sqrt{2}}\sigma_0 + \frac{1}{\sqrt{3}}\sigma_8 + \frac{1}{\sqrt{6}}\sigma_{15}, \qquad (51a)$$

$$\varphi_{\text{strange}} = \frac{1}{2}\sigma_0 - \sqrt{\frac{2}{3}}\sigma_8 + \frac{1}{2\sqrt{3}}\sigma_{15}, \qquad (51b)$$

$$\varphi_{\text{charm}} = \frac{1}{2}\sigma_0 - \frac{\sqrt{3}}{2}\sigma_{15}. \qquad (51c)$$

In these formulas φ_{strange} and φ_{charm} are the strange and charm quark condensate, respectively.

All models predict a qualitatively similar behavior for the temperature dependence of the up-down quark condensates. The strange quark condensate decreases more slowly with temperature than the up-down quark condensate. This is what one intuitively expects, as it appears more difficult to "melt" a condensate of heavier quark species than of light quark species.

Figure 4 shows the charm quark condensate. Note that this condensate is much larger than the other two condensates. A peculiar feature is that it first increases at a temperature of about 200 MeV, assumes a maximum at about 400 MeV, and then decreases. The maximum value is approxi-
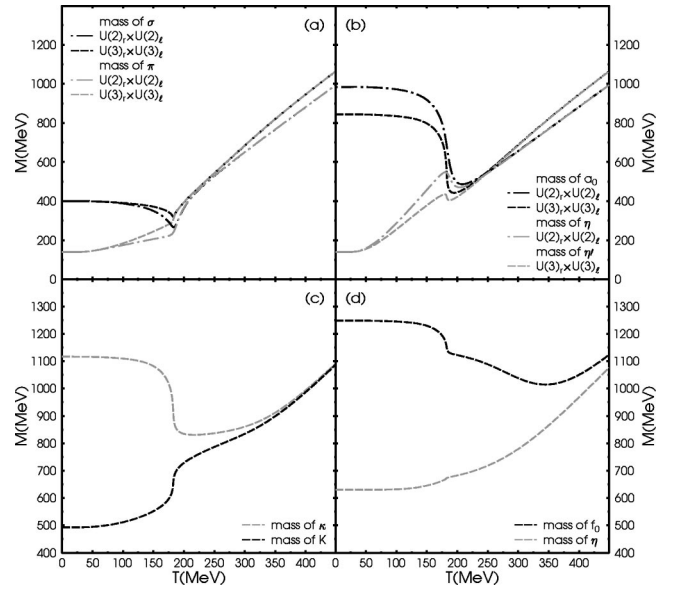

FIG. 5. The meson masses as a function of temperature for the different models in the case without the $U(1)_A$ anomaly and explicit chiral symmetry breaking.

mately 10% larger than the vacuum value. We are not aware of a simple explanation for this behavior.

B. Explicit chiral symmetry breaking without $U(1)_A$ anomaly

In Fig. 5 we show the masses for the scalar and pseudoscalar mesons for the case of explicit chiral symmetry breaking in the absence of the $U(1)_A$ anomaly. We discuss the results in comparison to the previous case. As in the previous case, the scalar meson masses stay constant up to temperatures close to the transition region, then decrease and finally start to increase again when they become degenerate with the pseudoscalar masses. In general, the pseudoscalar masses increase monotonously with temperature. The difference between the results obtained in the $U(2)_r \times U(2)_\ell$ and $U(3)_r \times U(3)_\ell$ model is rather small. An exception is the a_0 mass which is an input parameter in the former model, but is predicted in the latter.

A marked difference to the case with $U(1)_A$ anomaly is that the chiral symmetry restoration transition is much more
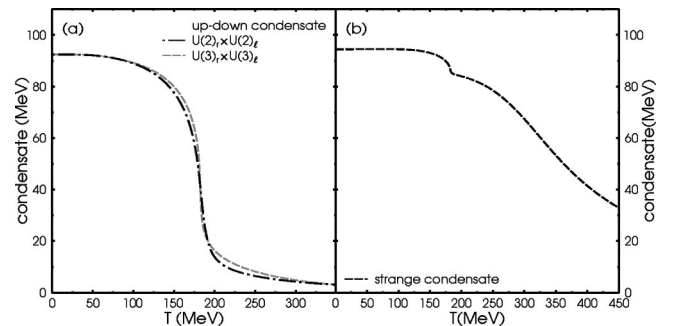

FIG. 6. (a) The up-down quark condensate and (b) the strange quark condensate as a function of temperature for the different models in the case without the $U(1)_A$ anomaly and explicitly broken chiral symmetry.
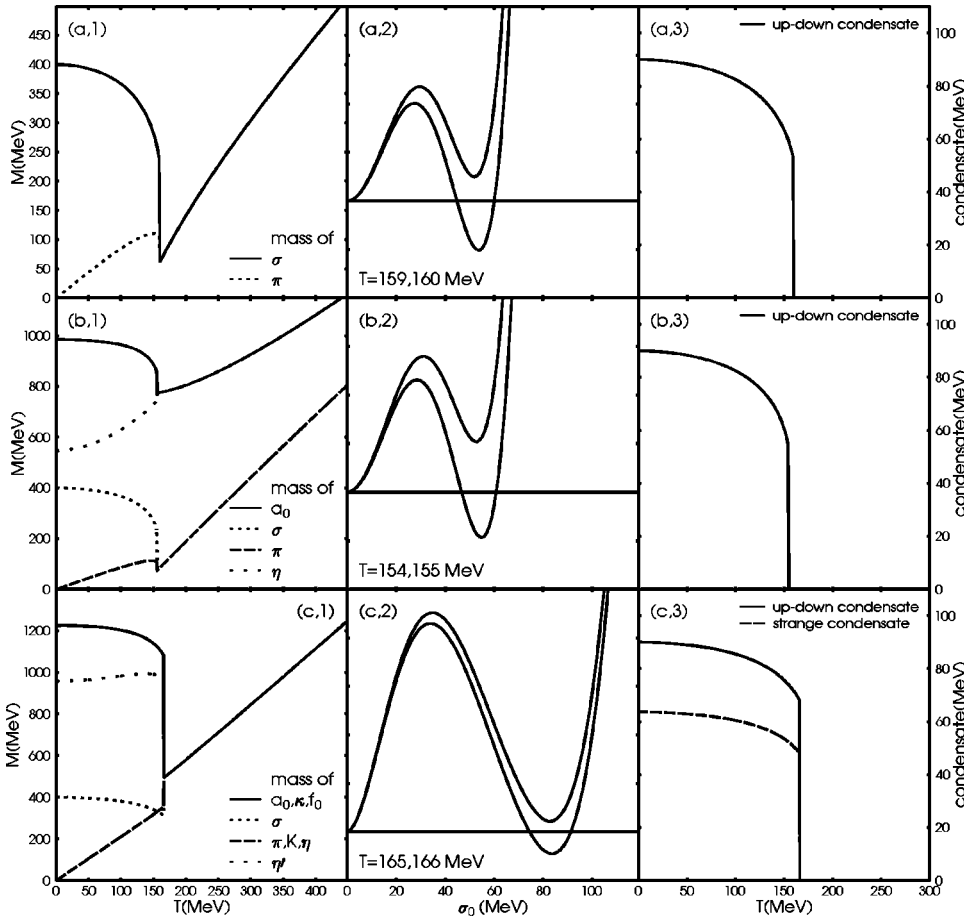
FIG. 7. The chiral limit with $U(1)_A$ anomaly. The temperature dependence of the meson masses are shown in panels (,1) and that of the up-down and strange quark condensates in panels (,3). The results for the $O(4)$ model are shown in panels (a,), for the $U(2)_r \times U(2)_\ell$ model in panels (b,), and for the $U(3)_r \times U(3)_\ell$ model in panels (c,). The effective potential (in arbitrary units) as a function of the condensate σ_0 is shown in panels (,2).

rapid, and it occurs at a slightly smaller temperature, $T \simeq 180$ MeV. Moreover, above the transition the scalar and pseudoscalar masses become degenerate much more rapidly. The reason is the absence of explicit $U(1)_A$ symmetry breaking. Another consequence of this is that, in the $U(2)_r \times U(2)_\ell$ model [the $U(3)_r \times U(3)_\ell$ model], the mass of the η meson (the η' meson) becomes degenerate with that of the pion at small and high temperatures. In the temperature range from about 50 MeV to 225 MeV, however, they are different. We believe this to be an artifact originating from the violation of Goldstone's theorem in the Hartree approximation, which becomes even more obvious when considering the chiral limit.

The melting of the condensates is shown in Fig. 6. The smaller transition temperature of about 180 MeV is also apparent in the temperature dependence of the up-down quark condensate. Again, the strange quark condensate melts less rapidly than the up-down quark condensate.

C. Chiral limit with $U(1)_A$ anomaly

The masses as a function of temperature for the $O(4)$ model are shown in Fig. 7(a,1), for the $U(2)_r \times U(2)_\ell$ model in Fig. 7(b,1), and for the $U(3)_r \times U(3)_\ell$ model in Fig. 7(c,1). In the $O(4)$ and $U(2)_r \times U(2)_\ell$ models, there are three Goldstone bosons, the pions, while in the $U(3)_r \times U(3)_\ell$ model there are eight Goldstone bosons, the pions, the kaons, and the η meson. The η' meson is not a

Goldstone boson due to the explicit breaking of the $U(1)_A$ symmetry by the anomaly. The scalar octet, comprising the three a_0 mesons, the four κ mesons, and the f_0 meson, is degenerate in mass, while the mass of the singlet σ differs from the mass of the octet. As the temperature increases, the scalar masses decrease while the pseudoscalar masses increase. The mass of the Goldstone bosons increases, because the Hartree approximation does not respect Goldstone's theorem at nonzero temperature [9,10].

Because of the restoration of chiral symmetry above the transition temperature T_c, the masses of the chiral partners become degenerate for temperatures $T > T_c$. For the $O(4)$ model, the chiral partners are the σ and the pion, for the $U(2)_r \times U(2)_\ell$ model they are the σ and the pion, as well as the a_0 and the η. Because of the explicit breaking of the $U(1)_A$ symmetry, the σ/pion and a_0/η do not become degenerate. The reason for this behavior is the term $\sim \mathcal{G}_{ab}$ in Eqs. (25). As discussed in Sec. III B, at zero temperature this term leads to a difference in the masses (squared) of the η meson and pion, and of the a_0 and σ meson, respectively, which is proportional to $2c$. In the case with the $U(1)_A$ anomaly, $2c \neq 0$ even for temperatures above T_c. Consequently, these mass differences persist also in the chirally restored phase.

For $N_f = 3$, the situation is different. The term $\sim \mathcal{G}_{ab}$ for $N_f = 2$ is replaced by a term $\sim \mathcal{G}_{abc}\sigma_c$. In the chirally symmetric phase, $\sigma_c = 0$, and consequently this term vanishes.
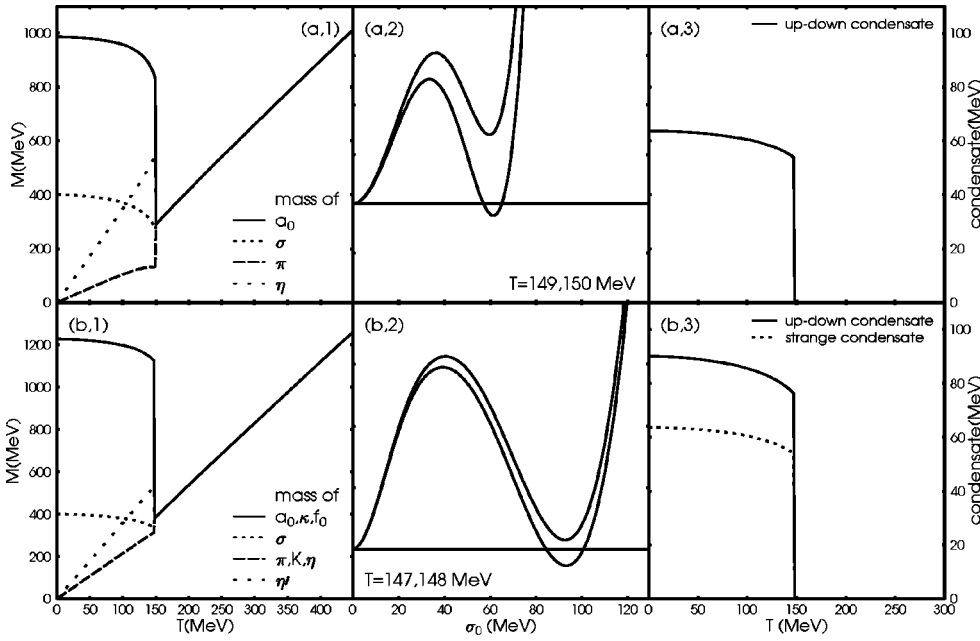
FIG. 8. The chiral limit without the $U(1)_A$ anomaly. The temperature dependence of the meson masses are shown in panels (,1) and that of the up-down and strange quark condensates in panels (,3). The results for the $U(2)_r \times U(2)_\ell$ model are shown in panels (a,), and for the $U(3)_r \times U(3)_\ell$ model in panels (b,). The effective potential (in arbitrary units) as a function of the condensate σ_0 is shown in panels (,2).

Therefore, all meson masses become degenerate, even in the case with the $U(1)_A$ anomaly.

All models exhibit a first order phase transition between the low-temperature phase where chiral symmetry is broken and the high-temperature phase where chiral symmetry is restored. For the $O(4)$ model and the $U(2)_r \times U(2)_\ell$ model with explicit breaking of the $U(1)_A$ symmetry, the transition should be of second order, cf. Sec. I. It is a known shortcoming of the Hartree approximation to predict a first order transition also in these cases. For the $U(2)_r \times U(2)_\ell$ model without explicit breaking of the $U(1)_A$ symmetry, and for all $U(N_f)_r \times U(N_f)_\ell$ models with $N_f > 2$ the transition is of first order, which is correctly reproduced by the Hartree approximation.

We have determined the numerical value of T_c by computing the effective potentials. The latter are shown for the three different models in the second column of Fig. 7 as a function of the condensate σ_0. (In the chiral limit, σ_0 is the only non-trivial condensate.) For the extraction of the transition temperature, the absolute normalization of the effective potential is irrelevant. All that matters is to identify the temperature where the minimum at the origin and the one at a non-zero value of σ_0 become degenerate. For this purpose we have plotted the effective potential for two temperatures, one slightly below and one slightly above T_c. From this we deduce that for the $O(4)$ model, Fig. 7(a,2), T_c is between 159 and 160 MeV. For the $U(2)_r \times U(2)_\ell$ model, Fig. 7(b,2), we obtain a critical temperature between 154 and 155 MeV. This temperature is rather close to the one in the $O(4)$ model. Finally, for the $U(3)_r \times U(3)_\ell$ model, the critical temperature is between 165 and 166 MeV, which is slightly larger than in the previous cases.

These values are surprisingly close to those obtained from lattice QCD calculations [4]. In the chiral limit, these calculations predict $T_c \simeq 175$ MeV for $N_f = 2$ and $T_c \simeq 155$ MeV for $N_f = 3$. The critical temperature obtained from the chiral models in the Hartree approximation deviates from these val-

ues only by about 20 MeV (or 12%) for $N_f = 2$ and only 10 MeV (or 6%) for $N_f = 3$. However, for the chiral models the transition temperature is larger in the three-flavor case than in the two-flavor case, while one finds the opposite behavior in the lattice QCD calculations.

For the sake of completeness we also show the condensates in the third column of Fig. 7. Note that, in contrast to the cases where chiral symmetry is explicitly broken, the strange condensate is smaller than the up-down condensate. The reason is that, in the chiral limit, $\sigma_8 = 0$, such that $\varphi_{\text{up-down}} = \sqrt{2}\,\varphi_{\text{strange}}$, cf. Eq. (50).

D. Chiral limit without $U(1)_A$ anomaly

The masses as a function of temperature are shown in Fig. 8(a,1) for the $U(2)_r \times U(2)_\ell$ model, and in Fig. 8(b,1) for the $U(3)_r \times U(3)_\ell$ model. In the first case, there are four Goldstone bosons, the pions and the η meson, while in the latter case there are nine Goldstone bosons, the pions, the kaons, and the η and η' mesons. As the temperature increases, the scalar masses decrease while the pseudoscalar masses increase, until they become degenerate in a first order phase transition. The mass of the Goldstone bosons increases with temperature, because the Hartree approximation does not respect Goldstone's theorem at nonzero temperature [9,10]. Moreover, the masses of the Goldstone bosons are not equal: for the $U(2)_r \times U(2)_\ell$ model, the η meson becomes heavier than the pion, while for the $U(3)_r \times U(3)_\ell$ model the η' meson becomes heavier than the other Goldstone bosons (pions, kaons, η meson). Note that the role of the η meson in the two-flavor case is assumed by the η' meson in the three-flavor case. The reason is that the physical meson corresponding to the singlet representation in the $U(2)_r \times U(2)_\ell$ model is the η meson, while it is the η' in the $U(3)_r \times U(3)_\ell$ model.

The numerical values for the critical temperature T_c have been determined by computing the effective potentials. The

latter are shown in the second column of Fig. 8 as a function of the condensate σ_0, for temperatures slightly below and above T_c. In the $U(2)_r \times U(2)_\ell$ model, Fig. 8(a,2), we obtain a critical temperature of $\simeq 150$ MeV. For the $U(3)_r \times U(3)_\ell$ model the temperature is slightly smaller, between 147 and 148 MeV. The ordering of critical temperatures for the two- and three-flavor cases is now reversed as compared to the case with the $U(1)_A$ anomaly, and is consequently in agreement with the ordering found in lattice QCD calculations. One might be tempted to view this as an indication for a rapidly decreasing $U(1)_A$ anomaly near the critical temperature, in agreement with the results of Ref. [25,26]. Finally, the condensates are shown in the third column of Fig. 8. The results are qualitatively similar to the case with the $U(1)_A$ anomaly.

V. CONCLUSIONS

In this work we have used several different chiral models, the $O(4)$, the $U(2)_r \times U(2)_\ell$, the $U(3)_r \times U(3)_\ell$, and the $U(4)_r \times U(4)_\ell$ linear sigma model, to compute the temperature dependence of meson masses and quark condensates across the chiral phase transition. The meson masses and condensates were self-consistently calculated in the Hartree approximation, which we derived via the CJT formalism. Moreover, we have studied several distinct patterns of symmetry breaking within the different models. For a list of cases studied here see Table I.

We first considered the physically relevant case of explicit symmetry breaking in the presence of the $U(1)_A$ anomaly and compared the results of the different chiral models in order to clarify how they change with the number of quark flavors N_f. Comparing the $O(4)$ model with the $U(2)_r \times U(2)_\ell$ model, one first notices that the degrees of freedom have doubled: in addition to the σ meson and the pions which are already present in the $O(4)$ model, one now has in addition the η meson and the a_0 mesons. This has the consequence that the meson masses grow more rapidly with temperature in the phase where chiral symmetry is restored. The reason for this are the tadpole contributions from the additional degrees of freedom to the meson self-energies, which lead to an increase in the meson masses. This result also applies when adding the strange degree of freedom in the framework of the $U(3)_r \times U(3)_\ell$ model. In fact, this picture holds in general, as long as the masses of the additional degrees of freedom are of the same order of magnitude as the chiral phase transition temperature. On the other hand, adding the heavy charm quark degree of freedom in the framework of the $U(4)_r \times U(4)_\ell$ model does not significantly influence the results for the masses of the non-charmed mesons and the non-charmed condensates. The reason is that the additional tadpole contributions from the heavy charmed mesons are exponentially suppressed with the meson mass, $\sim \exp(-M/T)$. Vice versa, also the masses of the charmed mesons do not change appreciably from their vacuum values over the range of temperatures of interest for chiral symmetry restoration, simply because the tadpole contributions from the non-charmed meson are small compared to the large vacuum mass of the charmed mesons. This result is intuitively clear from the physical point of view, but is still non-trivial: first, the equations for the in-medium masses are structurally different for the $U(4)_r \times U(4)_\ell$ model as compared to the $U(3)_r \times U(3)_\ell$ model. Second, the set of coupled equations for the masses and condensates is a nonlinear system of equations, which means that small perturbations could lead to large quantitative changes in the solution.

We then studied the case of explicit chiral symmetry breaking without a $U(1)_A$ anomaly. The main difference to the previous case was that the region of the chiral transition is narrower and located at a somewhat smaller temperature.

Finally, we considered the meson masses and quark condensates in the chiral limit. The Hartree approximation correctly predicts the chiral transition to be of first order in the $U(2)_r \times U(2)_\ell$ model without the $U(1)_A$ anomaly and in the $U(3)_r \times U(3)_\ell$ model. For the $O(4)$ model and the $U(2)_r \times U(2)_\ell$ model with the $U(1)_A$ anomaly the Hartree approximation incorrectly produces a first order instead of a second order phase transition. The transition temperatures are surprisingly close to the ones obtained in lattice QCD calculations. However, in the case with the $U(1)_A$ anomaly the transition temperature increases with the number of flavors, while in lattice QCD it decreases. This picture changes in the case without the $U(1)_A$ anomaly, where the transition temperature shows the same behavior with the number of quark flavors as in lattice QCD. This may indicate that the $U(1)_A$ symmetry is, at least partially, restored at and above the chiral phase transition temperature.

APPENDIX: SCALAR AND PSEUDOSCALAR MESON FIELDS

For $N_f = 2$, the identification of the physical scalar and pseudoscalar meson fields with the matrix fields defined in Eq. (19a) is

$$T_a \sigma_a = \frac{1}{\sqrt{2}} \begin{pmatrix} \frac{1}{\sqrt{2}}\sigma_0 + \frac{1}{\sqrt{2}}a_0^0 & a_0^+ \\ a_0^- & \frac{1}{\sqrt{2}}\sigma_0 - \frac{1}{\sqrt{2}}a_0^0 \end{pmatrix},$$

(A1a)

$$T_a \pi_a = \frac{1}{\sqrt{2}} \begin{pmatrix} \frac{1}{\sqrt{2}}\pi_0 + \frac{1}{\sqrt{2}}\pi^0 & \pi^+ \\ \pi^- & \frac{1}{\sqrt{2}}\pi_0 - \frac{1}{\sqrt{2}}\pi^0 \end{pmatrix}.$$

(A1b)

Here, $\pi^\pm \equiv (\pi_1 \mp i\pi_2)/\sqrt{2}$ and $\pi^0 \equiv \pi_3$ are the charged and neutral pions, respectively. Note the change of sign in the definition of the charged pion fields $\pi^\pm$ in terms of $\pi_{1,2}$ in comparison to Ref. [9]. The definition given here is the cor-

rect one, as one can readily confirm by writing the meson fields in terms of their quark content,

$$\pi_a \sim \bar{q} T_a \gamma_5 q. \tag{A2}$$

This applies also to the other charged meson fields defined in

the following. The field π_0 can be identified with the η meson. The parity partner of the pion is the $a_0(980)$ meson, i.e., $a_0^\pm \equiv (\sigma_1 \mp i\sigma_2)/\sqrt{2}$ and $a_0^0 \equiv \sigma_3$. The field σ_0 corresponds to the σ meson [now also referred to as $f_0(400 - 1200)$].

For $N_f = 3$ we obtain the following matrix:

$$T_a \sigma_a = \frac{1}{\sqrt{2}} \begin{pmatrix} \frac{1}{\sqrt{2}} a_0^0 + \frac{1}{\sqrt{6}} \sigma_8 + \frac{1}{\sqrt{3}} \sigma_0 & a_0^+ & \kappa^+ \\ a_0^- & -\frac{1}{\sqrt{2}} a_0^0 + \frac{1}{\sqrt{6}} \sigma_8 + \frac{1}{\sqrt{3}} \sigma_0 & \kappa^0 \\ \kappa^- & \bar{\kappa}^0 & -\frac{2}{\sqrt{3}} \sigma_8 + \frac{1}{\sqrt{3}} \sigma_0 \end{pmatrix}, \tag{A3a}$$

$$T_a \pi_a = \frac{1}{\sqrt{2}} \begin{pmatrix} \frac{1}{\sqrt{2}} \pi^0 + \frac{1}{\sqrt{6}} \pi_8 + \frac{1}{\sqrt{3}} \pi_0 & \pi^+ & K^+ \\ \pi^- & -\frac{1}{\sqrt{2}} \pi^0 + \frac{1}{\sqrt{6}} \pi_8 + \frac{1}{\sqrt{3}} \pi_0 & K^0 \\ K^- & \bar{K}^0 & -\frac{2}{\sqrt{3}} \pi_8 + \frac{1}{\sqrt{3}} \pi_0 \end{pmatrix}. \tag{A3b}$$

The fields $K^\pm \equiv (\pi_4 \mp i\pi_5)/\sqrt{2}$, $K^0 \equiv (\pi_6 - i\pi_7)/\sqrt{2}$, and $\bar{K}^0 \equiv (\pi_6 + i\pi_7)/\sqrt{2}$ are the kaons. In general, because the strange quark is much heavier than the up or down quarks, the π_0 and the π_8 are admixtures of the η and the η' meson. We identify the parity partner of the kaon with the κ meson [now referred to as $K_0^*(1430)$ in [24]]. Finally, in general the σ_0 and the σ_8 are admixtures of the σ and $f_0(980)$ mesons.

For $N_f = 4$ the following identification of physical fields with matrix elements holds:

$$T_a \sigma_a = \frac{1}{\sqrt{2}} \begin{pmatrix} A_S & a_0^+ & \kappa^+ & \bar{D}_0^0 \\ a_0^- & B_S & \kappa^0 & D_0^- \\ \kappa^- & \bar{\kappa}^0 & C_S & D_{s,0}^- \\ D_0^0 & D_0^+ & D_{s,0}^+ & D_S \end{pmatrix}, \tag{A4}$$

where

$$A_S = \frac{1}{2} \sigma_0 + \frac{1}{\sqrt{2}} a_0^0 + \frac{1}{\sqrt{6}} \sigma_8 + \frac{1}{\sqrt{12}} \sigma_{15},$$

$$B_S = \frac{1}{2} \sigma_0 - \frac{1}{\sqrt{2}} a_0^0 + \frac{1}{\sqrt{6}} \sigma_8 + \frac{1}{\sqrt{12}} \sigma_{15},$$

$$C_S = \frac{1}{2} \sigma_0 - \frac{2}{\sqrt{6}} \sigma_8 + \frac{1}{\sqrt{12}} \sigma_{15},$$

$$D_S = \frac{1}{2} \sigma_0 - \frac{3}{\sqrt{12}} \sigma_{15},$$

and

$$T_a \pi_a = \frac{1}{\sqrt{2}} \begin{pmatrix} A_P & \pi^+ & K^+ & \bar{D}^0 \\ \pi^- & B_P & K^0 & D^- \\ K^- & \bar{K}^0 & C_P & D_s^- \\ D^0 & D^+ & D_s^+ & D_P \end{pmatrix}, \tag{A5}$$

with

$$A_P = \frac{1}{2} \pi_0 + \frac{1}{\sqrt{2}} \pi^0 + \frac{1}{\sqrt{6}} \pi_8 + \frac{1}{\sqrt{12}} \pi_{15},$$

$$B_P = \frac{1}{2} \pi_0 - \frac{1}{\sqrt{2}} \pi^0 + \frac{1}{\sqrt{6}} \pi_8 + \frac{1}{\sqrt{12}} \pi_{15},$$

$$C_P = \frac{1}{2} \pi_0 - \frac{2}{\sqrt{6}} \pi_8 + \frac{1}{\sqrt{12}} \pi_{15},$$

$$D_P = \frac{1}{2} \pi_0 - \frac{3}{\sqrt{12}} \pi_{15}.$$

Here, $D^0 = (\pi_9 + i\pi_{10})/\sqrt{2}$, $\bar{D}^0 = (\pi_9 - i\pi_{10})/\sqrt{2}$, $D^\pm = (\pi_{11} \pm i\pi_{12})/\sqrt{2}$, and $D_s^\pm = (\pi_{13} \pm i\pi_{14})/\sqrt{2}$ are the charged and neutral pseudoscalar mesons with charm quantum numbers. The π_0, π_8, and π_{15} fields are admixtures of the η, η', and η_c mesons. The charged and neutral scalar mesons with charm quantum numbers are $D_0^0 = (\sigma_9 + i\sigma_{10})/\sqrt{2}$, $\bar{D}_0^0 = (\sigma_9 - i\sigma_{10})/\sqrt{2}$, $D_0^\pm = (\sigma_{11} \pm i\sigma_{12})/\sqrt{2}$, and $D_{s,0}^\pm = (\sigma_{13} \pm i\sigma_{14})/\sqrt{2}$. These scalar mesons have not been identified experimentally, yet. The σ_0, σ_8, and σ_{15} fields are admixtures of the σ, f_0, and χ_{c0} mesons.

---

[1] G. 't Hooft, Phys. Rev. D **14**, 3432 (1976).
[2] G. 't Hooft, Phys. Rev. Lett. **37**, 8 (1976).
[3] R.D. Pisarski and F. Wilczek, Phys. Rev. D **29**, 338 (1984).
[4] F. Karsch, Lect. Notes Phys. **583**, 209 (2002).
[5] F.R. Brown *et al.*, Phys. Rev. Lett. **65**, 2491 (1990).
[6] Y. Iwasaki, K. Kanaya, S. Kaya, S. Sakai, and T. Yoshie, Z. Phys. C **71**, 343 (1996).
[7] J.T. Lenaghan, Phys. Rev. D **63**, 037901 (2001).
[8] L. Dolan and R. Jackiw, Phys. Rev. D **9**, 3320 (1974).
[9] J.T. Lenaghan, D.H. Rischke, and J. Schaffner-Bielich, Phys. Rev. D **62**, 085008 (2000).
[10] J.T. Lenaghan and D.H. Rischke, J. Phys. G **26**, 431 (2000).
[11] M. Gell-Mann and M. Levy, Nuovo Cimento **16**, 705 (1960).
[12] N. Petropoulos, J. Phys. G **25**, 2225 (1999).
[13] J.M. Cornwall, R. Jackiw, and E. Tomboulis, Phys. Rev. D **10**, 2428 (1974).
[14] H. van Hees and J. Knoll, Nucl. Phys. **A683**, 369 (2000).
[15] H. van Hees and J. Knoll, Phys. Rev. D **65**, 025010 (2002).
[16] H. van Hees and J. Knoll, Phys. Rev. D **65**, 105005 (2002).
[17] H. van Hees and J. Knoll, Phys. Rev. D **66**, 025028 (2002).
[18] R. Jackiw, Phys. Rev. D **9**, 1686 (1974).
[19] M. Levy, Nuovo Cimento A **52**, 23 (1967).
[20] B. Hu, Phys. Rev. D **9**, 1825 (1974).
[21] J. Schechter and M. Singer, Phys. Rev. D **12**, 2781 (1975).
[22] H.B. Geddes, Phys. Rev. D **21**, 278 (1980).
[23] C. Vafa and E. Witten, Nucl. Phys. **B234**, 173 (1984).
[24] Particle Data Group, K. Hagiwara *et al.*, Phys. Rev. D **66**, 010001 (2002).
[25] B. Alles, M. D'Elia, and A. Di Giacomo, Nucl. Phys. **B494**, 281 (1997).
[26] J. Schaffner-Bielich, Phys. Rev. Lett. **84**, 3261 (2000).